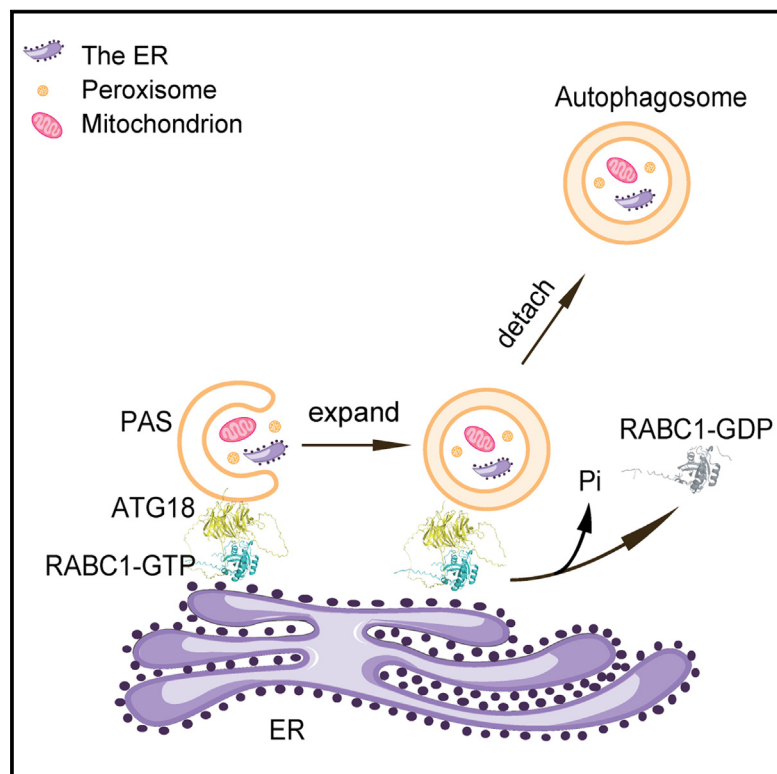


An Arabidopsis Rab18 GTPase promotes autophagy by tethering ATG18a to the ER in response to nutrient starvation

Graphical abstract



Authors

Jiaqi Sun, Yang Shao,
Songyang Wang, ..., Pierre Leroy,
Chengyang Li, Huanquan Zheng

Correspondence

jiaqi.sun@sdu.edu.cn (J.S.),
hugo.zheng@mcgill.ca (H.Z.)

In brief

The regulation of autophagy in plant response to stresses is not well defined. Sun and Shao et al. have found that RABC1, an Arabidopsis Rab18, interacts with and recruits ATG18a to the ER to facilitate autophagosome expansion on the ER in plant response to nutrient starvation.

Highlights

- In *rabc1* mutant cells, autophagy is compromised under nutrient starvation
- RABC1 plays a role in autophagosome expansion in response to nutrient starvation
- Active RABC1 specifically interacts with ATG18a
- RABC1 regulates ER association of ATG18a and its subsequent detachment from the ER

Article

An Arabidopsis Rab18 GTPase promotes autophagy by tethering ATG18a to the ER in response to nutrient starvation

Jiaqi Sun,^{1,2,4,*} Yang Shao,^{1,4} Songyang Wang,¹ Xunzheng Li,¹ Shuqing Feng,¹ Wein Wang,² Pierre Leroy,² Chengyang Li,³ and Huanquan Zheng^{2,5,*}

¹Key Laboratory of Plant Development and Environmental Adaptation Biology, Ministry of Education, School of Life Sciences, Shandong University, Qingdao 266237, Shandong, China

²Department of Biology, McGill University, Montreal, QC H3B 1A1, Canada

³Key Laboratory of Horticultural Plant Biology, Ministry of Education, Huazhong Agricultural University, Wuhan 430070, Hubei, China

⁴These authors contributed equally

⁵Lead contact

*Correspondence: jiaqi.sun@sdu.edu.cn (J.S.), hugo.zheng@mcgill.ca (H.Z.)

<https://doi.org/10.1016/j.devcel.2023.11.006>

SUMMARY

The expansion of autophagosomes requires a controlled association with the endoplasmic reticulum (ER). However, the mechanisms governing this process are not well defined. In plants, ATG18a plays a key role in autophagosome formation in response to stress, yet the factors regulating the process are unknown. This study finds that ATG18a acts as a downstream effector of RABC1, a member of the poorly characterized Rab18/RabC GTPase subclass in plants. Active RABC1 interacts with ATG18a on the ER, particularly under nutrient starvation. In *rabc1* mutants, autophagy is compromised, especially under nutrient deprivation, affecting the ER association and expansion of ATG18a-positive autophagosomes. Furthermore, both dominant-negative and constitutively active RABC1 forms inhibit autophagy. The dominant inactive RABC1 impedes the ER association of ATG18a, whereas the constitutively active RABC1 delays ATG18a detachment from the ER. Collectively, RABC1 regulates the ER association and the subsequent detachment of ATG18a-positive autophagosomes during nutrient starvation.

INTRODUCTION

Rab GTPases constitute the largest family of Ras-like small GTPases in eukaryotic cells. They are the master regulators of various membrane trafficking pathways in the endomembrane system. Rab GTPases function as molecular switches mainly in the tethering of transport vesicles to the targeting membranes but are also involved in the formation, transport, docking, and fusion of transport vesicles during membrane trafficking.¹ A Rab GTPase cycles between inactive guanosine diphosphate (GDP)-bound form and active guanosine triphosphate (GTP)-bound form through the exchange of GTP and GDP via interactions with Rab GEFs (guanine nucleotide exchange factors) and Rab GAPs (GTPase activating proteins).² In the active GTP-bound form, Rab GTPases recruit their downstream effectors to coordinate membrane trafficking. Once the action is completed, the active GTP-bound form switches to the GDP-bound form; therefore, its activity is turned off.

In Arabidopsis, at least 57 Rab GTPases have been identified, which are divided into 8 distinct clades—RabA to RabH.^{1,3} The primary functions of most clades of Arabidopsis Rab GTPases in membrane trafficking have been defined in plant development, hormone signaling, cell-wall biosynthesis, and stress re-

sponses,^{1,4,5} except for the RabC clade, whose functions remain elusive. In Arabidopsis, there are 3 RabCs—RABC1, RABC2a, and RABC2b.³ RabCs are homologs of mammalian Rab18.³ Mammalian Rab18 is found in a wide range of tissues and cell lines in mouse.⁶ Solid evidence now exists that Rab18 plays a crucial role in animal and human development, yet the exact molecular roles Rab18 plays are still not well defined owing to the complicated subcellular localizations revealed in different cell types.⁷ Studies over the past 30 years have provided evidence that Rab18 plays a role in endocytic transport in polarized epithelial cells,⁸ in endoplasmic reticulum (ER)-Golgi transport,⁹ in the morphology of the ER,¹⁰ lipid droplets (LD),¹¹ and most recently in autophagy by promoting autolysosome maturation.¹²

Autophagy is a conserved cellular process for the continuous renovation of cytoplasmic components through the degradation of damaged/dysfunctional components/organelles either under basal condition or in response to external stress.¹³ For instance, the damaged/dysfunctional ER can be targeted by selective autophagy for degradation, a process termed ER-phagy.^{14–16} In plants, numerous stresses, including carbon starvation, salt stress, and ER stress, can induce ER-phagy.^{17,18} In autophagy, damaged/dysfunctional components/organelles, including the ER (cargoes), are encased in the autophagosome, a double-membrane

structure generated by a series of dedicated processes, including the initiation, expansion, and closure of a cup-shaped membrane. Autophagosomes are then matured and fused to lysosome/vacuole for cargo degradation.^{19,20} The regulation of autophagy is highly conserved in eukaryotic cells, and more than 40 conserved autophagy-related (ATG) proteins have been identified.^{21,22} For example, the Atg1 kinase promotes the nucleation of autophagosomes. Atg8, a ubiquitin-like protein, is crucial for the expansion of autophagosomes, which requires the action of the Atg5-Atg12-Atg16 E3-like ligase complex.^{13,23,24} There is a complex interplay between the autophagosome expansion and the ER. The ER serves as a membrane source for the autophagosome expansion.²⁵ In mammalian cells, Atg18 plays a role in the tethering of autophagosomes to the ER.²⁶ Yet, how the activity of Atg18 is modulated is not known. In plants, ATG18 is crucial for autophagy, including ER-phagy in plant responses to nutrient deficiency, salt stress, oxidative stress, ER stress, and drought.^{27–30} ATG18a has a phospholipid binding ability that is important for the growth of autophagosomes,³¹ yet it is not known if plant ATG18 associates with the ER for the expansion of autophagosomes.

A recent study in plants has suggested an interesting role of RABC1 in stomatal development.³² It is reported that when plants are treated oleic acid, an LD inducer, RABC1 in guard cells momentarily relocates to the surface of LDs. The absence of RABC1 leads to a deficiency in LD mobilization in guard cells when treated with oleic acid. Given that RABC1 is ubiquitously expressed in plant tissues,³³ it is possible that RABC1 performs additional functions in plants. We reported here that RABC1 plays a role in plant response to nutrient (carbon and nitrogen) starvation during seedling growth. We revealed that RABC1 is localized to the ER and autophagosomes. It promotes autophagy in plant response to nutrient starvation but not under ER stress. We demonstrated that Arabidopsis ATG18a is associated with the ER. Active RABC1 specifically interacts with ATG18a and promotes the association of ATG18a to the ER and therefore the expansion of ATG18a-positive autophagosomes in autophagy.

RESULTS

***rabc1* mutant is hypersensitive to nutrient starvation but not ER stress**

In order to determine what function RABC1 might have in plants, we first identified an intron transfer DNA (T-DNA) insertional *rabc1* line (SALK_012129) (Figure S1A), which exhibited a significantly reduced expression of the *RABC1* gene (Figure S1B). It is worth noting that the same Salk line was reported as a knockout line.³² The *RABC1* gene is expressed ubiquitously in various tissues³³ (Figures S1C and S1D). We found that, in comparison with wild type (WT), *rabc1* only displayed a subtle growth defect during seedling growth under normal conditions on 1/2 Murashige Skoog (MS) medium containing 1% sucrose (Figure 1A). However, under the carbon starvation condition on 1/2 MS medium without sucrose supply, the growth of *rabc1* seedlings was significantly affected (Figure 1A). There were ~50% of seedlings that turned yellow or died (Figures 1A and 1B). Moreover, we conducted a transient carbon starvation experiment involving 5-day-old seedlings grown on 1/2 MS medium supplemented with sucrose, which were subsequently transferred to 1/2 MS medium devoid of sucrose and kept in darkness. Compared with WT seedlings, *rabc1* mutant

seedlings displayed a notable yellowing phenotype within 10 days (Figures 1C and S1F). Additionally, upon transferring normal-grown seedlings to nitrogen-deficient 1/2 MS medium, *rabc1* mutant seedlings exhibited a brownness phenotype resembling that of *atg5-1* mutant seedlings, which was in contrast to the appearance of WT seedlings (Figure 1C). Expression of YFP-RABC1 under either the native or the 35S promoter in the *rabc1* mutant rescued the growth defect of *rabc1* on the 1/2 MS medium without sucrose or under the transient carbon starvation treatment (Figures 1A, 1B, S1E, and S1F). We then conducted an investigation into the expression level of *RABC1* during carbon starvation. We revealed a transient upregulation of the *RABC1* expression within 4 to 12 h, followed by a decline after 24 h (Figure S1G). Interestingly, we found that, although *atg5-1* was hypersensitive to dithiothreitol (DTT) (ER stress inducer) treatment, *rabc1* showed no obvious difference from WT when treated with DTT (Figures 1D and 1E), suggesting that RABC1 has a specific role in plant response to nutrient (carbon and nitrogen) starvation but not to ER stress.

RABC1 is localized to the ER, Golgi, and autophagy compartments

In order to comprehend the cellular basis of the function of RABC1 in the plant response to nutrient starvation, we investigated the subcellular localization of RABC1 in the rescued *rabc1* lines expressing YFP-RABC1. In addition to being found in the cytoplasm (Figure 2A), YFP-RABC1 was also partially targeted to the ER indicated by mCherry-HDEL (Figure 2A, arrows). Additionally, RABC1 was noticeable in a number of punctae, using mCherry-ATG8e as a marker, we found that some of RABC1 punctae, especially those in the cytoplasmic region of cells, were localized to autophagosomes (Figure 2B, arrows), and some of them were localized to ATG18a-positive autophagosomes (Figure 2C, arrows). In addition, some of punctae, especially those relatively large ones, were co-localized with ST (sialyltransferase)-RFP (Figure 2D), A Golgi marker. When transiently expressed in *N. benthamiana* leaves, YFP-RABC1 distributed similarly to YFP-RABC1 in rescued *rabc1* (Figures S2A–S2C). They were co-localized with the ER (Figure S2A, arrows), some punctae were co-localized with autophagosomes (Figure S2B, arrows), and some were co-localized with Golgi (Figure S2C, arrows) marked by ST-RFP. However, none of them were co-localized with Mito-mCherry (mitochondria) (Figure S2D) or PX-mCherry (peroxisome) (Figure S2E).

RABC1 promotes autophagic flux

Next, we investigated the potential cellular function of RABC1 by the classic dominant-negative (SN)/constitutively active (QL) approach.³⁴ In the dominant-negative approach, a Rab is locked in GDP-binding state, which strongly binds and thus interferes with the action of its GEF(s). In the constitutively active approach, a Rab is locked in GTP-binding form, which exhibits sustained/unregulated activation, thus also allowing researchers to investigate the function of a Rab on cellular processes.¹ Because RABC1 is targeted to the ER and Golgi, we first wondered whether RABC1 is involved in ER-Golgi trafficking. When ST-RFP was co-expressed with YFP-RABC1(S27N), a dominant-negative form of RABC1, and YFP-RABC1(Q71L), a constitutively active form of RABC1, Golgi targeting of ST-RFP was not affected (Figures S2F and S2G), suggesting that RABC1 does not play a role in

Developmental Cell

Article

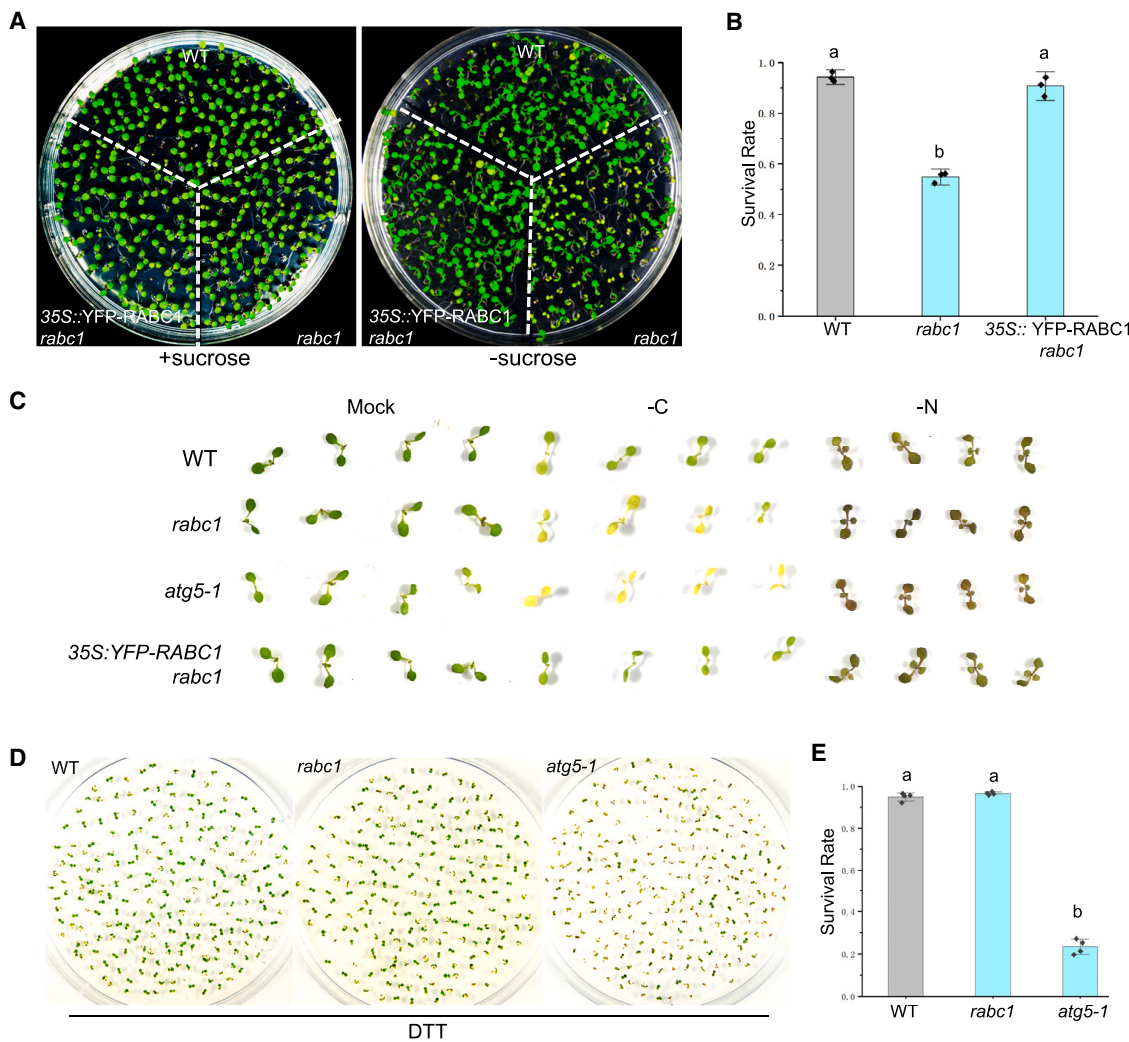


Figure 1. *rabc1* mutant is hypersensitive to nutrient starvation but not ER stress

(A) Seedlings of wild type (WT), *rabc1*, and 35S::YFP-RABC1 *rabc1* grown on 1/2 MS with (the left side) or without (the right side) sucrose for 7 days.

(B) The quantification of survival rate of seedlings grown without sucrose (A). Each time, about 120 seedlings were quantified, and 3 repeats were performed. Error bars represent mean ± SD. Different letters indicate statistically significant differences (ANOVA, Fisher's least significant difference test, $p < 0.05$).

(C) Seedlings of WT, *rabc1*, *atg5-1*, and 35S::YFP-RABC1 *rabc1* grown on 1/2 MS with sucrose for 7 days, moved to 1/2 MS without sucrose and kept in the dark (-C), or moved to 1/2 MS without nitrogen (-N) for 10 days.

(D) 7-day-old seedlings of WT, *rabc1*, and *atg5-1* grown on 1/2 MS in the presence of 1 mM DTT.

(E) The quantification of survival rate of (D). Each time, about 200 seedlings were quantified, and 4 repeats were performed. Error bars represent mean ± SD. Different letters indicate statistically significant differences (ANOVA, Fisher's least significant difference test, $p < 0.05$).

See also Figure S1.

ER-Golgi trafficking. We also noticed that dominant-negative YFP-RABC1(S27N) was mainly cytosolic (Figure S2F), whereas constitutively active YFP-RABC1(Q71L) was cytosolic, as well as on punctae larger than average YFP-RABC1 punctae (compare Figure S2G with Figure S2C). None of the YFP-RABC1(Q71L) punctae were co-localized with ST-RFP (Figure S2G). To investigate the potential involvement of RABC1 in the post-Golgi trafficking pathway, we conducted a co-expression experiment involving Sec-mCherry along with YFP-RABC1, YFP-RABC1(S27N), or YFP-RABC1(Q71L). Sec-mCherry is a mCherry variant that is secreted into the apoplast, and if the post-Golgi trafficking process is impaired, Sec-mCherry should be visible in the interior of the

cell.³⁴ However, we observed no retention of sec-mCherry inside cells in the presence of RABC1 variants (Figure S3). This observation suggests that RABC1 may not play a significant role in the post-Golgi trafficking pathway.

We then co-expressed mCherry-ATG8e together with free YFP, YFP-RABC1, YFP-RABC1(S27N), or RABC1(Q71L), and the number of autophagosomes was quantified. In the presence of YFP-RABC1, there were more mCherry-ATG8e punctae than that in the presence of YFP only (compare Figure 3B with Figures 3A and 3E), and many mCherry-ATG8e punctae were co-localized with YFP-RABC1 (Figure 3B). Fewer mCherry-ATG8e punctae were observed in the presence of

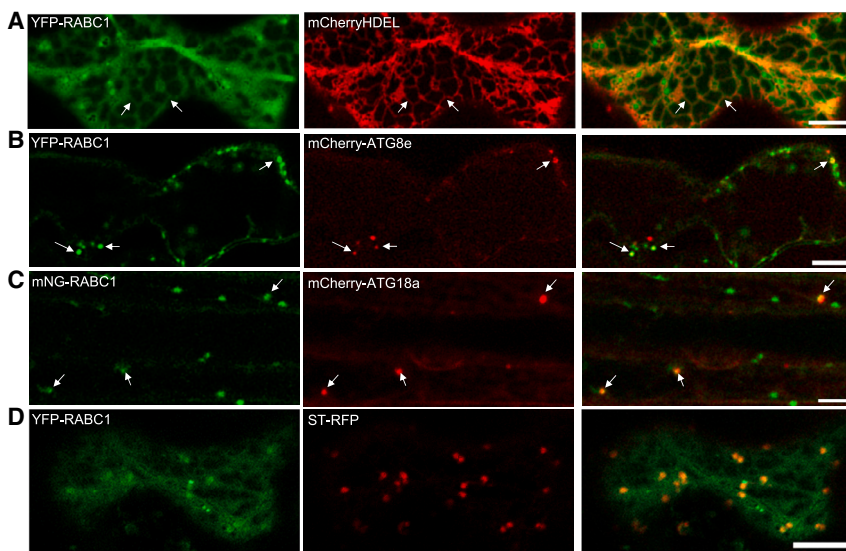


Figure 2. Subcellular localization of RABC1

(A) RABC1 is partially localized to the ER marked by mCherryHDEL. Seedlings expressing both YFP-RABC1 driven by the 35S promoter and mCherryHDEL were used for imaging. Arrows indicate RABC1 (shape line) on the ER. Scale bars: 10 μm.
(B) RABC1 is partially localized to autophagosomes marked by mCherry-ATG8e. Seedlings expressing both YFP-RABC1 driven by the 35S promoter and mCherry-ATG8e were used for imaging. Arrows indicate the co-localization between YFP-RABC1 and mCherry-ATG8. Scale bars: 10 μm.
(C) RABC1 is partially localized to ATG18a-positive autophagosomes. Seedlings expressing both mNeonGreen-RABC1 driven by the native RABC1 promoter and mCherry-ATG18a were used for imaging. Arrows indicate the co-localization between mNeonGreen-RABC1 and mCherry-ATG18a. Scale bars: 10 μm.

(D) RABC1 is partially localized to Golgi. Seedlings expressing both YFP-RABC1 driven by the native RABC1 promoter, and ST-RFP were used for imaging. Scale bars: 10 μm.

See also [Figure S2](#).

RABC1(S27N) or YFP-RABC1(Q71L) than in the presence of YFP (compare [Figures 3C](#) and [3D](#) with [Figures 3A](#) and [3E](#)). In the case of YFP-RABC1(Q71L), YFP-RABC1(Q71L) punctae were not co-localized with mCherry-ATG8e punctae ([Figure 3D](#)). These results suggested that the formation of autophagosomes is promoted by YFP-RABC1 but inhibited by YFP-RABC1(S27N) and YFP-RABC1(Q71L). Furthermore, we found that mCherry cleavage of mCherry-ATG8e was also promoted in the presence of YFP-RABC1 (compare lane 2 with lane 1 in [Figures 3F](#) [top] and [3G](#)) but inhibited in the presence of YFP-RABC1(S27N) or YFP-RABC1 (Q71L) (compare lane 3–4 with lane 1 in [Figures 3F](#) [top] and [3G](#)). Moreover, we also observed an impaired efficiency of YFP cleavage in YFP-RABC1(S27N) and YFP-RABC1(Q71L) mutants, compared with WT YFP-RABC1 ([Figures 3F](#) [lower] and [3H](#)). Together, these data indicated that RABC1 promotes autophagic flux.

To further confirm this notion, we investigated the impact of the expression of different versions of RABC1 on ER-phagy using mCherry-TMC (transmembrane domain and C-terminal tail of the yeast Sey1p protein). We have previously reported that the ER membrane marker TMC is excellent for monitoring ER-phagy both microscopically and biochemically.^{35–37} Co-expression of HA-RABC1 with mCherry-TMC resulted in an enhanced flux of ER-phagy, as evidenced by an increased number of mCherry-TMC punctae within the vacuole in the presence of the cysteine protease inhibitor E64d ([Figures S4A](#) and [S4B](#)) and a more pronounced cleaved free mCherry band ([Figures S4C](#) and [S4D](#)). Conversely, when HA-RABC1(S27N) and HA-RABC1(Q71L) mutants were present, the efficiency of ER-phagy was found to be inhibited both microscopically ([Figures S4A](#) and [S4B](#)) and biochemically ([Figures S4C](#) and [S4D](#)). These findings confirm that RABC1 promotes autophagic flux.

RABC1 promotes carbon-starvation-induced autophagy, including ER-phagy

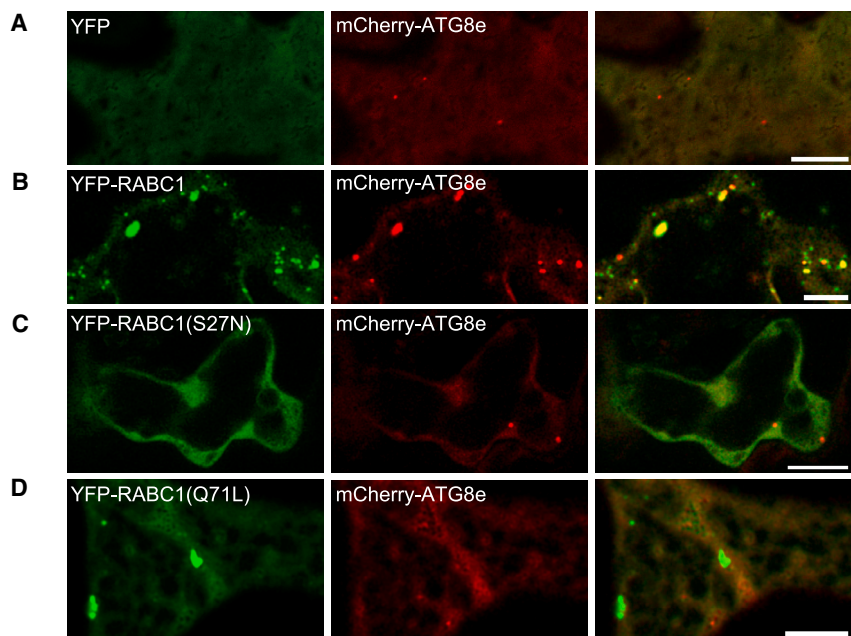
Because *rabc1* is hypersensitive to nutrient (carbon and nitrogen) starvation but not ER stress, we wondered how autophagy

may be affected in *rabc1* under either nutrient deficient or ER stress. To this end, we examined ER-phagy under carbon starvation and ER stress because it was reported that both carbon starvation and ER stress induce ER-phagy in plants.^{18,30} First of all, we wondered if YFP-RABC1 is targeted, along with the ER (mCherryHDEL) to the vacuole by autophagy in carbon starvation treatment using concanamycin A (ConcA). ConcA is a specific inhibitor of the V-ATPase activity that inhibits acidification of the vacuole, promoting the accumulation of autophagic bodies for YFP visualization.³⁸ After a 6-h carbon-starvation treatment, YFP-RABC1 punctae were clearly visible in the vacuole and were partially co-localized with mCherryHDEL-labeled punctae in cells of the transgenic plants co-expressing YFP-RABC1 and mCherryHDEL ([Figure 4B](#), arrows). In mock samples, neither YFP-RABC1 nor mCherryHDEL was seen in the vacuole ([Figure 4A](#)). The result indicates that YFP-RABC1, together with mCherryHDEL is transported to the vacuole. The YFP-RABC1 punctae observed were co-localized with mCherry-ATG8e within the vacuole following carbon starvation ([Figure S5A](#)), indicating that these punctae are autophagic bodies. Intriguingly, the DTT treatment triggered ER-phagy as shown by the accumulation of mCherryHDEL in the vacuole ([Figure 4C](#), arrows), but few YFP-RABC1 were found co-localized with mCherryHDEL punctae in the vacuole ([Figure 4C](#), arrowhead). Similarly, we observed minimal co-localization between YFP-RABC1 and mCherry-ATG8e following DTT treatment, suggesting that RABC1 specifically promotes carbon-starvation-induced but not DTT-induced ER-phagy. This notion was further supported by our quantification, which revealed that there were more YFP-RABC1 punctae ([Figure 4D](#)) and stronger association of YFP-RABC1 with mCherryHDEL punctae ([Figure 4E](#)) in cells under carbon starvation than that treated with DTT ([Figures 4D](#) and [4E](#)).

Subsequently, we compared the cleavage efficiency of free YFP from YFP-RABC1 in cells under carbon starvation and DTT treatment. We found that the cleavage of free YFP from YFP-RABC1 in WT was enhanced under carbon starvation

Developmental Cell

Article



E

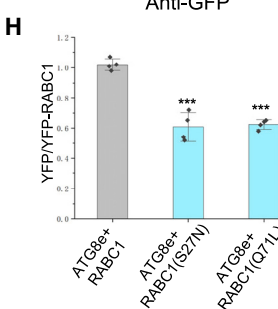
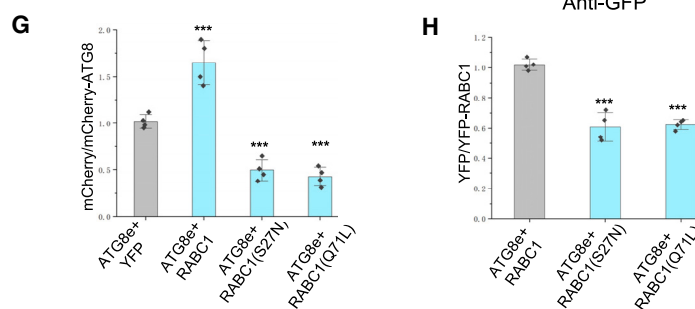
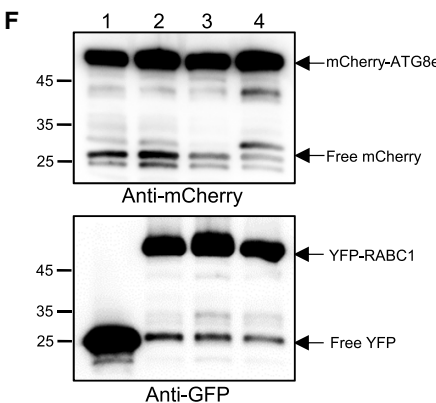
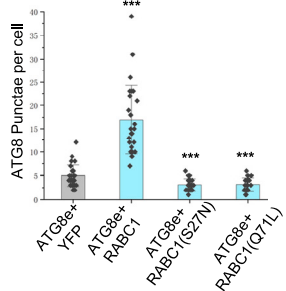


Figure 3. RABC1 promotes autophagic flux

(A–D) Transient co-expression of mCherry-ATG8e with YFP (A), YFP-RABC1 (B), YFP-RABC1(S27N) (C), or YFP-RABC1(Q71L) (D) in *N. benthamiana* leaves. Scale bars: 10 μ m.

(E) The quantification of the number of mCherry-ATG8e punctae in (A)–(D). Error bars represent SD, and *** represents significant difference from the YFP control ($p < 0.001$).

(F) Western blot of total proteins extracted from (A) to (D) samples with anti-mCherry (the upper blot) and anti-GFP (the lower blot). Lane (1–4): mCherry-ATG8e + YFP (1), mCherry-ATG8e + YFP-RABC1 (2), mCherry-ATG8e + YFP-RABC1(S27N) (3), and mCherry-ATG8e + YFP-RABC1(Q71L) (4).

(G) The quantification of the ratio between free mCherry and mCherry-ATG8 in (F). Error bars represent mean \pm SD, *** represents significant difference from the YFP control ($p < 0.001$).

(H) The quantification of the ratio between free YFP and YFP-RABC1 in (F). Error bars represent mean \pm SD, *** represents significant difference from the YFP control ($p < 0.001$).

See also Figures S3 and S4.

RABC1 relies on conventional autophagy pathway. In summary, a greater amount of RABC1 is directed to the vacuole for degradation by autophagy together with the ER during carbon starvation but not under DTT treatment.

To further confirm that RABC1 plays a role in the ER-phagy, we employed YFP-TMC to compare the efficiency of ER-phagy in *rabc1* grown under carbon starvation with DTT treatment. The YFP cleavage from YFP-TMC was significantly increased in WT plants under carbon starvation treatment (Figure 4H). In comparison, the YFP cleavage efficiency was compromised in the *rabc1* mutant under carbon starvation (Figure 4H). By contrast, both WT and *rabc1* mutant plants treated with DTT had almost identical YFP cleavage efficiency of YFP-TMC (Figure 4I). Moreover, our microscopy data aligned very well with these biochemical data, showing that there was a significant reduction in YFP-TMC punctae within the vacuole of *rabc1* mutant cells following carbon starvation but not during ER stress induced by TM (Figures S5C and S5D).

Finally, in *rabc1* treated with carbon starvation, we observed compromised degradation not only of an ER protein (BIP2) but also of peroxisomal and mitochondrial proteins (PEX12 and CYC1, respectively) in *rabc1* mutants (Figures S5E–S5H). This observed impairment of protein degradation across multiple organelle proteins indicates that RABC1 extends its role beyond ER-phagy and encompasses a broader function in autophagy in general.

(Figure 4F), but not under DTT treatment (Figure 4G). We further compared YFP-RABC1 cleavage under tunicamycin (TM), another ER stress inducer that inhibits protein glycosylation in the ER³⁹ to that under DTT and carbon starvation. We found that only carbon starvation but not DTT nor TM promoted cleavage of YFP-RABC1 (Figure S5B), suggesting that RABC1 plays an exclusive role in response to carbon starvation rather than in response to ER stress induced by either TM or DTT. Furthermore, no significantly increased cleavage of free YFP from YFP-RABC1 was observed in *atg5-1* under carbon starvation (Figure 4F), suggesting that the cleavage of YFP from YFP-

TMC punctae within the vacuole of *rabc1* mutant cells following carbon starvation but not during ER stress induced by TM (Figures S5C and S5D).

Finally, in *rabc1* treated with carbon starvation, we observed compromised degradation not only of an ER protein (BIP2) but also of peroxisomal and mitochondrial proteins (PEX12 and CYC1, respectively) in *rabc1* mutants (Figures S5E–S5H). This observed impairment of protein degradation across multiple organelle proteins indicates that RABC1 extends its role beyond ER-phagy and encompasses a broader function in autophagy in general.

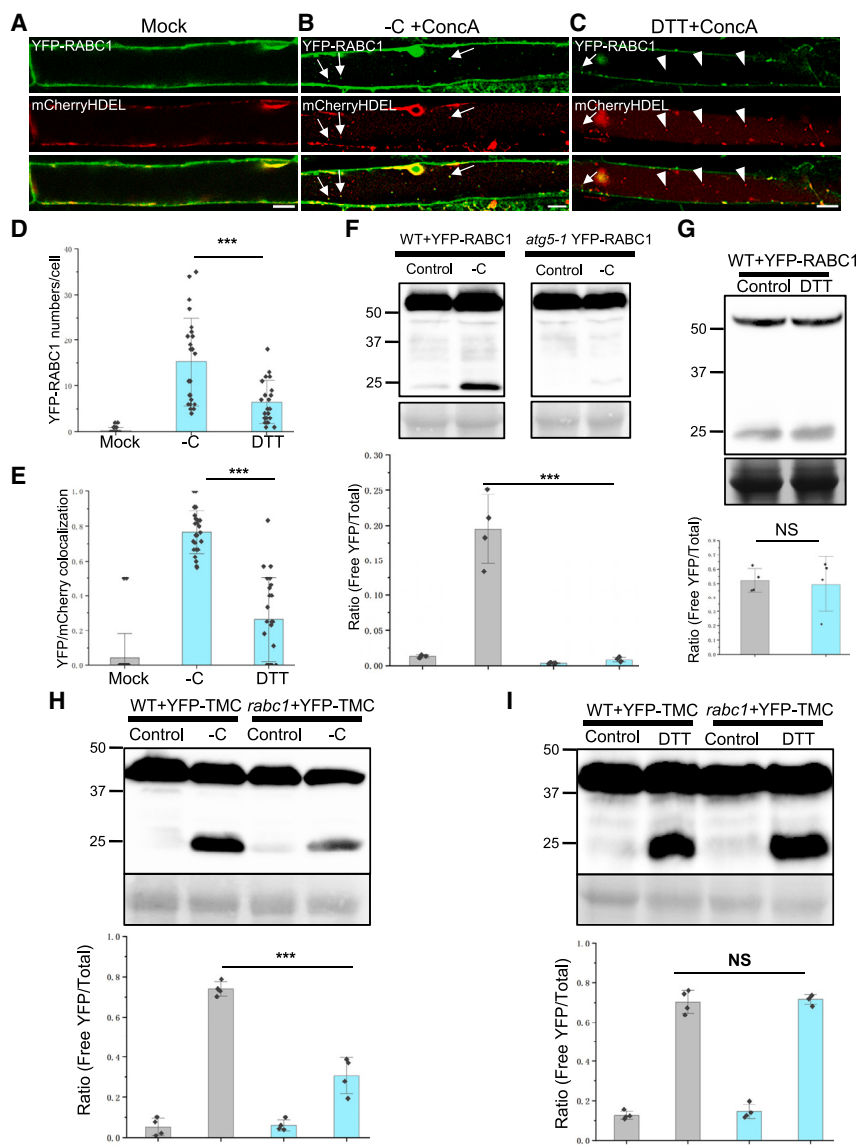


Figure 4. RABC1 promotes carbon-starvation-induced autophagy including ER-phagy

(A–C) Confocal imaging of the middle section cells from 5-day-old *rabc1* seedlings expressing YFP-RABC1 and mCherryHDEL after being treated with liquid MS with DMSO (mock) (A), carbon starvation + ConcA (B), or with DTT + ConcA (C). Arrows in (B) and (C) point the co-localization of YFP-RABC1 and mCherryHDEL punctae in the vacuole, and arrowheads in (C) point mCherryHDEL punctae in the vacuole that are not with YFP-RABC1. Scale bars: 10 μ m.

(D) The quantification of the number of YFP-RABC1 punctae in (A)–(C). The number of YFP-RABC1 within the vacuole (in the middle focus of each cell) was quantified. Error bars represent SD, and *** represents significant difference ($p < 0.001$).

(E) The quantification of the percentage of YFP-RABC1 co-localized with mCherryHDEL punctae in (A)–(C). Error bars represent SD, and *** represents significant difference ($p < 0.001$).

(F) Western blot of total proteins extracted from 5-day-old WT (top left image) or *atg5-1* (top right image) seedlings expressing YFP-RABC1 treated with carbon starvation for 12 h. Ponceau S staining was used as the loading control. The bottom graph indicates the cleavage efficiency of free YFP quantified. Error bars represent SD, and *** represents significant difference ($p < 0.001$).

(G) Western blot of total proteins extracted from 5-day-old WT seedlings expressing YFP-RABC1 treated with 2 mM DTT for 12 h. Coomassie blue staining was used as the loading control. The bottom graph shows the cleavage efficiency of free YFP quantified. Error bars represent SD, and NS represents no significant different ($p > 0.05$).

(H and I) Western blot of total proteins extracted from 5-day-old WT or *rabc1* seedlings expressing YFP-TMC treated with carbon starvation for 12 h (H) or with 2 mM DTT for 12 h (I). Ponceau S staining was used as the loading control. The bottom graphs in (H) and (I) show the cleavage efficiency of free YFP quantified. Error bars represent SD, and *** represents significant difference ($p < 0.001$, t test). NS represents no significant different ($p > 0.05$).

See also Figure S5.

Active RABC1 specifically interacts with ATG18a on the ER

To determine how RABC1 is involved in autophagy, we proceeded to investigate whether RABC1 interacts with any of the autophagy-related (ATG) core proteins by performing co-immunoprecipitation (coIP). When YFP-RABC1 was co-expressed with mCherry-ATG8e, mCherry-ATG18a, and mCherry-ATG5, only mCherry-ATG18a was efficiently co-purified with YFP-RABC1. By contrast, neither mCherry-ATG8e nor mCherry-ATG5 exhibited such interactions (Figure 5A). Furthermore, *in vitro* pull-down experiment revealed that ATG18a interacted with WT RABC1 and had an even stronger interaction with constitutively active form of RABC1 (Q71L) but did not interact with dominant-negative form of RABC1(S27N) (Figure 5B). Furthermore, we also observed a significant enhancement of the interaction between RABC1 and ATG18a following carbon starvation but not ER stress

(Figures 5C and 5D). This result indicated that the RABC1-ATG18a interaction is finely modulated by specific cellular stress conditions. Using BiFC (Bimolecular fluorescence complementation), we found that RABC1 interacted with ATG18a near (Figure 5E, row 1, arrowhead) or on the ER (Figure 5E, row 1, arrow). Our quantification found that 60% of BiFC punctae were on the ER (Figure 5F). Remarkably, over 85% of the interactions between RABC1(Q71L) and ATG18a took place on the ER (Figure 5E, row 2, arrows, and 5F). RABC1(S27N) did not interact with ATG18a (Figure 5E, row 3). There were no interactions revealed in cVenus and nVenus controls either (Figure S6A, rows 1–4). The specific interaction of ATG18a with WT and constitutively active RABC1(Q71L) suggested that ATG18a might be an effector protein of RABC1. Moreover, we performed a 3D structural simulation of ATG18a and RABC1 based on the Alphafold database and found that the contact between ATG18a and RABC1

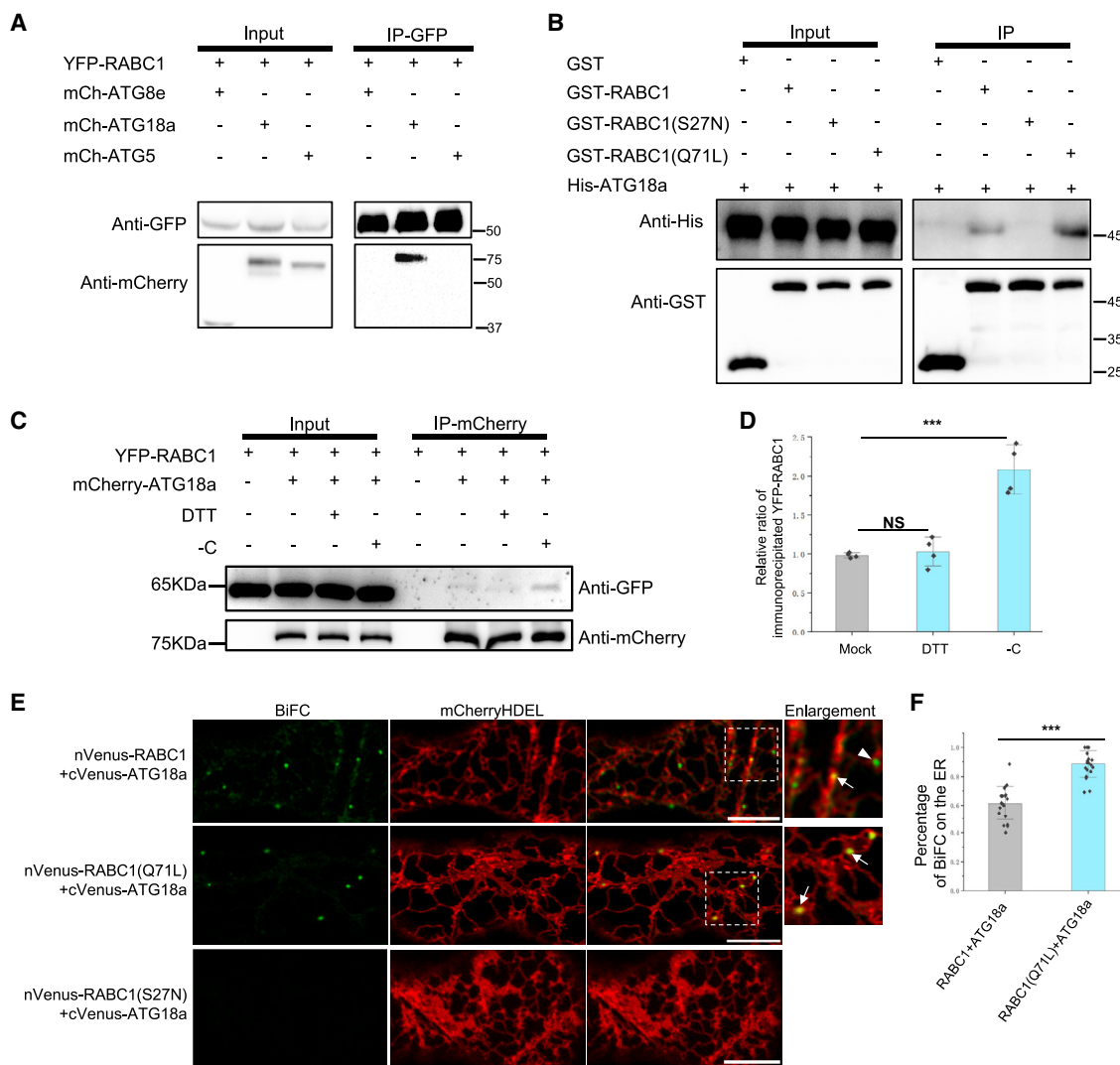


Figure 5. Active RABC1 interacts specifically with ATG18a

- (A) Co-immunoprecipitation of mCherry-ATG8e, mCherry-ATG18a, and mCherry-ATG5 with YFP-RABC1. Only mCherry-ATG18a (lane 2), but not mCherry-ATG8 (lane 1) nor mCherry-ATG5 (lane 3) was co-purified with YFP-RABC1.
- (B) *In vitro* protein interaction test between His-ATG18a and GST-RABC1, GST-RABC1(S27N), or GST-RABC1(Q71L). His-ATG18a interacts with GST-RABC1 and GST-RABC1(Q71L) but not with GST-RABC1(S27N).
- (C) Co-immunoprecipitation of YFP-RABC1 and mCherry-ATG18a expressed in seedlings subjected to indicated treatments, including mock control, DTT treatment, and carbon starvation. Co-immunoprecipitation experiments were conducted using anti-mCherry beads. Seedlings expressing YFP-RABC1 were used as the negative control.
- (D) Relative ratio of immunoprecipitated YFP-RABC1 by mCherry-ATG18a quantified in (C). Error bars represent mean \pm SD, *** represents significant difference ($p < 0.001$). NS represents no significant difference ($p > 0.05$).
- (E) BiFC analysis of the interaction between ATG18a and RABC1. Scale bars: 10 μ m. Arrows indicate the co-localization between YFP-RABC1 and mCherry-ATG8. The arrowhead indicates the presence of punctate that are not associated with the ER.
- (F) The quantification of BiFC signals on the ER from (E). BiFC signals in each cell (from 20 cells) were quantified, and experiments were repeated three times. Error bars represent SD, and *** represents significant difference ($p < 0.001$).

See also [Figure S6](#).

may be mediated by the hydrogen bond between Ser311 (on ATG18a) and Asn36 (on RABC1) ([Figures S6B and S6C](#)).

RABC1 regulates the growth of ATG18a structures

ATG18a participates in the expansion of autophagosomes.^{31,40} Next, we investigated how RABC1 might act on ATG18a in the expansion of autophagosomes. To this end, we expressed

mNeonGreen-ATG18a in WT and *rabc1*, and we found that ATG18a punctae were smaller and more in number in *rabc1* mutant cells than that in WT cells under carbon starvation, but there was no significant difference in the mock control ([Figure 6A](#)). This notion was supported by our quantification of the size ([Figure 6B](#)) and the number ([Figure 6C](#)) of ATG18a punctae. Similarly, when compared with WT, we saw a reduction in size

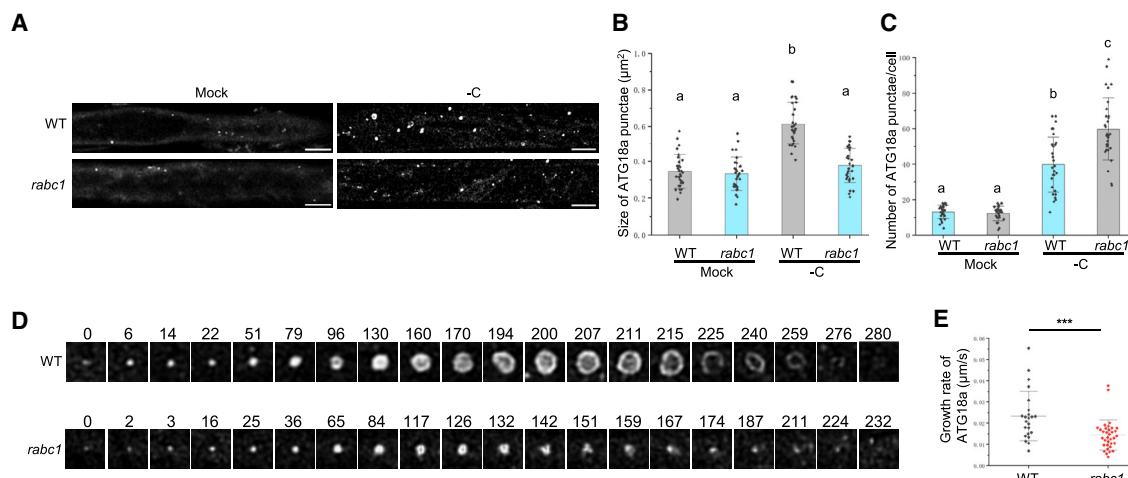


Figure 6. The growth of ATG18a-positive autophagosomes is defective in rabc1 mutant

(A) Confocal analysis of cells of WT (top two images) or rabc1 (bottom two images) seedlings expressing UBQ10pro::mNeonGreen-ATG18a in the mock control (left two images) and under carbon starvation (-C) (right two images). Scale bars: 10 μ m.

(B and C) The quantification of the size (B) and number (C) of ATG18a-positive autophagosomes in WT and rabc1. Error bars represent SE, and *** represents significant difference ($p < 0.001$). About 25 cells were quantified for WT or rabc1.

(D) Living imaging of the growth of an ATG18a-positive autophagosome in WT and rabc1. The time units indicated are seconds.

(E) The quantification of the growth rate of ATG18a-positive autophagosomes in WT and rabc1. Error bars represent SD, and *** represents significant difference ($p < 0.001$).

See also Figure S7.

and an increase in the number of ATG18a punctae in the rabc1 mutant under nitrogen starvation, whereas no significant difference in the size and number of ATG18a punctae was observed under ER stress (Figures S7A–S7C). Detailed live imaging of the growth of mNeonGreen-ATG18a punctae revealed that, in WT cells, many ATG18a punctae formed, grew, and became fully expanded in 200 s (Figure 6D). Subsequently, they started to decay and quickly disappeared after around 250–280 s (Figure 6D). In rabc1 cells, many of ATG18a punctae did not become well expanded before they started to decay and eventually disappeared within 230 s (Figure 6D). Our quantification of the growth rate of ATG18a punctae revealed that the growth of ATG18a punctae in WT cells was 0.023 μ m²/s in average (Figure 6E). In rabc1, it was reduced to 0.014 μ m²/s (Figure 6E). We also quantified the lifetime of ATG18a punctae in WT and rabc1 cells. We found that there was no significant difference between WT and rabc1 (Figure S7D). Taken all together, we conclude that RABC1 regulates the expansion of ATG18a-positive autophagosomes.

RABC1 plays a role in tethering ATG18a to the ER

Atg18 has been reported to tether pre-autophagosomal membrane to the ER and facilitate the lipid transfer for autophagosome formation in mammalian cells,²⁶ although it is not known if Arabidopsis ATG18a plays a similar role or not. Because RABC1 regulates the expansion of ATG18a punctae, and ATG18a may be an effector protein of RABC1, we wondered if ATG18a is tethered to the ER and if RABC1 plays a role in tethering ATG18a to the ER for autophagosome expansion. In order to investigate these, we first co-expressed mNeon-Green-ATG18a and mScarletHDEL in both WT and in rabc1. Our analysis of projected image stacks over 5 μ m revealed

that a large portion of mNeonGreen-ATG18a punctae were located on the ER in WT cells (Figure 7A, arrows), whereas many mNeonGreen-ATG18a punctae were found off the ER in rabc1 mutant cells (Figure 7A, arrowheads). Our quantification revealed that in WT cells, there were more than 60% ATG18a punctae on the ER, whereas in rabc1 cells there were only less than 40% ATG18a punctae on the ER (Figure 7B). Furthermore, our TEM analysis also revealed a higher abundance of unclosed autophagosome structures that were smaller in rabc1 cells than that in WT (Figure S7E, arrows). Notably, a significant proportion of these observed autophagosomes in rabc1 mutant cells appeared to be away from the ER (Figure S7E). The result collectively indicated that ATG18a is tethered to the ER, and RABC1 plays a role in tethering ATG18a to the ER.

Subsequently, we transiently co-expressed mNeonGreen-ATG18a and mCherryHDEL with HA-RABC1, HA-RABC1(S27N), and HA-RABC1(Q71L) in the *N. benthamiana* leaves to compare the different effects between the WT and two mutant forms of RABC1. Similar expression of HA-RABC1, HA-RABC1(S27N), and HA-RABC1(Q71L) was confirmed by western blot (Figure 7F). Compared with HA-RABC1 (Figure 7C), in the presence of HA-RABC1(S27N), more mNeonGreen-ATG18a signal was retained in the cytosol, with fewer but smaller mNeonGreen-ATG18a punctae associated with the ER (Figure 7D, arrowheads). This was verified by quantifying the size of ATG18a punctae, the ratio of ATG18a punctae/cytosol signal, and the percentage of ER-associated ATG18a punctae (Figures 7G–7I). It is interesting that in the presence of HA-RABC1(Q71L), although the ratio of ATG18a punctae/cytosol signal was similar to that in HA-RABC1 (compare Figure 7E with Figures 7C and 7H), mNeonGreen-ATG18a punctae in the presence of HA-RABC1(Q71L) appeared lesser in

Developmental Cell

Article

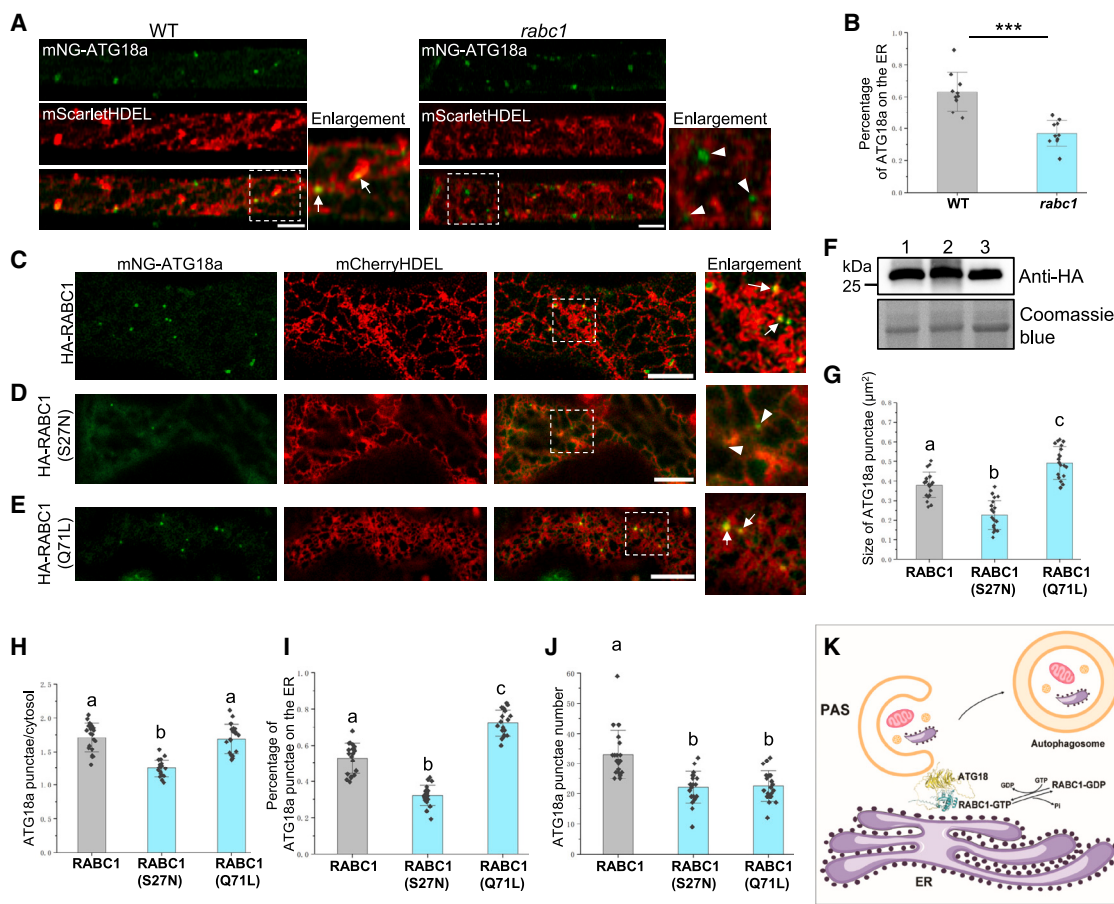


Figure 7. RABC1 plays a role in tethering ATG18a to the ER

(A) The projection of confocal images of WT and *rabc1* seedlings expressing mNeonGreen-ATG18a and mScarletHDEL. Arrows point mNeonGreen-ATG18a punctae on the ER, and arrowheads point mNeonGreen-ATG18a punctae off the ER. Scale bars: 10 μm .

(B) The percentage of ATG18a punctae on the ER in WT and *rabc1* quantified. Error bars represent SD, and *** represents significant difference ($p < 0.001$).

(C–E) Confocal imaging of mNeonGreen-ATG18a and mCherryHDEL transiently co-expressed with HA-RABC1 (C), HA-RABC1(S27N) (D), or HA-RABC1(Q71L) (E). Arrows point mNeonGreen-ATG18a punctae on the ER, and arrowheads point at mNeonGreen-ATG18a punctae off the ER. Scale bars: 10 μm .

(F) The expression levels of HA-tagged RABC1 variants in (C)–(E) assessed using anti-HA. Lines 1, 2, and 3 represent (C)–(E), respectively.

(G–J) The size (G) of ATG18a punctae, the ratio of ATG18a punctae to cytosolic signal (H), the percentage of ATG18a punctae on the ER (I) and the number of ATG18a punctae (J) were quantified in the presence HA-RABC1, HA-RABC1(S27N), and HA-RABC1(QL) as observed in (C)–(E). The non-punctate and diffusing signal was defined as cytosolic signal. Error bars represent SD. Different letters indicate statistically significant differences (ANOVA, Fisher's least significant difference test, $p < 0.05$).

(K) Proposed working model for RABC1 in autophagy. Inactive GDP-RABC1 is normally in the cytosol. GDP-RABC1 recruited onto the ER is activated with a switch to GTP-RABC1. Active GTP-RABC1 on the ER interacts with and tethers ATG18a to the ER so autophagosomes are expanded on the ER. The expansion is likely facilitated by material transfer from the ER. At a certain point, active GTP-RABC1 is turned off by GTP hydrolysis. Inactive GDP-RABC1 is recycled back to the cytosol, and expanding autophagosomes are detached from the ER for further expansion or maturation.

number but larger in size than that in HA-RABC1 (compare Figure 7E with Figures 7C, 7G, and 7J). More mNeonGreen-ATG18a in presence of HA-RABC1(Q71L) were associated with ER (Figure 7E, arrows) than that in the presence of WT RABC1, which was supported by the quantification (Figure 7I). Taken all together, we conclude that RABC1 serves as one of the molecules that governs the tethering of ATG18a to the ER, as well as the subsequent detachment of ATG18a from the ER.

DISCUSSION

Despite of recent advances in our knowledge of the actions of different Rab GTPases, the precise cellular function of RabC

Rab18 is not well defined both in plant and in mammalian cells. Here, we report that Arabidopsis RABC1, a member of the RabC clade, is required for plant responses to nutrient (carbon and nitrogen) starvation. RABC1 is localized in the cytosol and in multiple cellular compartments, including the ER, Golgi, and autophagosomes. However, RABC1 does not appear to participate in ER-Golgi and post-Golgi transport processes. Instead, it is primarily involved in autophagy triggered by nutrient deficiency. We find that active RABC1 specifically interacts with ATG18a, either on or near the ER, whereas inactive RABC1 does not display such interaction. In addition, the interaction between RABC1 and ATG18a is enhanced by carbon starvation but not in response to ER stress. It is interesting that the expression

of *RABC1* is also transiently upregulated by carbon starvation. In *rabc1* mutant cells, the ER association of ATG18a is impaired in nutrient-deficient conditions, leading to reduced size and the growth rate of ATG18a. Therefore, we propose that RABC1 promotes nutrient starvation-induced autophagy, including ER-phagy, by tethering ATG18a to the ER to facilitate the expansion of ATG18a-positive autophagosomes (Figure 7K). This promotion is likely a result of the enhanced interaction between RABC1 and ATG18a, along with transient upregulation of the *RABC1* gene expression. Ge et al.³² recently reported that RABC1 contributes to the mobilization of LDs during stomatal development.³² Upon being treated with oleic acid, an LD formation inducer, RABC1 is transiently localized to the LDs in guard cells where it recruits AtSEIPIN2 as an effector, a stomatal-specific protein involved in LD development.³² However, it remains unclear whether RABC1 functions in a similar manner in the absence of oleic acid or in tissues other than stomata. Notably, RABC1 is ubiquitously expressed in plant tissues. Furthermore, autophagy is known to be involved in making LD contents accessible to the cell.⁴¹ Therefore, it is possible that the LD mobilization defect observed in the *rabc1* mutant is explained by defective autophagy revealed here. In this regard, Ge et al.³² reported that aberrantly enlarged LDs present in *rabc1* mutant cells, a sign that the degradation of LDs is defective in *rabc1* mutant cells.

It is known that the expansion of autophagosomes requires a supply of membrane materials from the ER. In yeast and mammalian cells, the Atg18-Atg2 complex tethers growing autophagosomes to the ER, facilitating the lipid transfer from the ER to autophagosomes.^{26,40} However, the existence of any factor(s) that facilitate the tethering of ATG18-ATG2 to the ER is unknown. In plants, ATG18a is crucial for the formation of autophagosomes under a variety of stress conditions.^{28,29,42} Nonetheless, the specific mechanisms by which ATG18a is involved in this process and how its actions are regulated remain unclear. Our findings provide insights into these questions by demonstrating that ATG18a is associated with the ER and is a downstream effector of RABC1. The ER association of ATG18a is facilitated by active RABC1 on the ER. We note that, in *rabc1* mutant cells, the ER association of ATG18a is not completely blocked, and potentially, the residual expression of *RABC1* in the knockdown *rabc1* mutant contributes to the still observed association. However, it is also possible that there are additional mechanisms for ER-autophagosome association; therefore, the linkage between ATG18a and the ER still operates in *rabc1*, although less effectively. For example, it has been recently reported in plants that VAMP724 (Vesicle Associated Membrane Protein724) and VAMP726, two soluble N-ethylmaleimide-sensitive factor attachment protein receptor (SNARE) proteins, work together with ATG9 in regulating autophagosome progression from the ER.^{43,44} The lipid-binding protein ORP2A interacts with VAMP-associated protein (VAP)27-1 to mediate ER-autophagosomal membrane contact for autophagy.⁴⁵ These pathways may compensate the ER-autophagosome association defect when RABC1 is defective. As such, autophagy in the *rabc1* mutant is not completely blocked.

To regulate membrane trafficking precisely, a Rab protein continually cycles between active and inactive forms, allowing its activity to be turned on and off in a timely manner. In *rabc1* mutant cells, there are more but smaller ATG18a-labeled autophagosomes but fewer ATG8-positive autophagosomes. A similar

ATG18a phenotype is also observed when persulfidation of ATG18a, which is important for the phospholipid binding of ATG18a, is disrupted.³¹ It is noteworthy that overexpression of dominant active form of RABC1 leads to an enhanced ER association of ATG18a, as well as enlarged ATG18a punctae, whereas it reduces the number of ATG8 punctae. Yet, dominant active RABC1 does not co-localize with ATG8e. Our interpretation of these results is that ATG18a is the direct effector of RABC1, whereas ATG8 acts in the subsequent step. It has been shown that ATG8 is recruited after ATG18a is nucleated, but ATG8 is co-localized with ATG18a for around 60 s during the formation of autophagosomes.³¹ Because constitutively active RABC1 cannot be turned off, it would lead to a prolonged ER retention of ATG18a-positive autophagosomes, thus potentially delaying their detachment from the ER. This would result in enlarged ATG18a-positive autophagosomes but fewer ATG8-positive autophagosomes as the secondary effect. Therefore, RABC1 is a master regulator of ATG18a, controlling the loading of ATG18a to the ER for expansion and its subsequent detachment from the ER for further expansion or maturation (Figure 7K).

Autophagy is one of the cellular mechanisms plant cells use to respond to various stresses.^{18,31} It is noteworthy that RABC1 promotes carbon-starvation-induced autophagy including ER-phagy, but it does not participate in ER-phagy induced by ER stress. In plants, the protein kinase TOR (target of rapamycin) regulates autophagy induced by nutrient starvation, salt, and osmotic stress but not autophagy induced by ER stress or oxidative stress.⁴⁶ Therefore, it is possible that the action of RABC1-ATG18a in autophagy, including ER-phagy under nutrient starvation, is TOR signaling pathway dependent. Although TOR-regulated autophagy is dependent on ATG18a,⁴⁷ ATG18a is reported to be involved in ER-phagy induced by ER stress.^{30,31,46} Thus, TOR may modulate the action of RABC1-ATG18a through RABC1. Indeed, we found that the AZD8055 (a TOR inhibitor) treatment significantly increased the size and number (doubled in average) of ATG18a punctae in WT. In the *rabc1* mutant, only ~60% increase in the size of ATG18a punctae was observed along with a greater increase (tripled in average) in the number of ATG18a punctae in response to the AZD8055 treatment (Figures S7F–S7H).

Last but not least, ER-phagy is a highly selective process mediated by specific ER-phagy receptors. In plants, several ER-phagy receptors have been recently identified. AtSec62, a constituent of the protein translocator in the ER, is an ER-phagy receptor required for ER stress tolerance.¹⁷ Two ATG8-interacting proteins, ATI1 and ATI2, have been shown to function as ER-phagy receptors in plant responses to carbon starvation.¹⁸ C53, a soluble protein, also serves as an ER-phagy receptor when ribosomes stall on the ER under ER stress.⁴⁸ Most recently, it has been shown that RHD3 serves as an ER-phagy receptor to alleviate ER stress.³⁵ It will be interesting to examine if RABC1 works together with any of the ER-phagy receptors under the carbon starvation condition.

Limitations of the study

Although our research has elucidated a role of RABC1 in facilitating the attachment of ATG18a to the ER and its subsequent detachment from the ER during autophagy, several critical questions remain unanswered. It remains to be determined what other factors are involved in the ER association of ATG18a in autophagy in plant cells. In mammalian cells, the ULK1/FIP200-VAPs

Developmental Cell

Article



complex is known to play a role in ER contact of WIPI2/Atg18.⁴⁹ In addition, it is not clear whether RABC1 also collaborates with ATG9, another membrane supplier for autophagosome expansion. Moreover, the mechanisms that activate and recruit RABC1 to the ER in plant response to nutrient starvation remain incompletely understood. Our data suggest that the action of RABC1 in autophagy is under the regulation of the TOR signaling pathway. It would be interesting to examine if and how TOR may interplay with the guanine exchange factor of RABC1³² to gain crucial insights into this regulation. Additionally, it is not clear whether RABC1 also collaborates with selective autophagy receptors for degradation of the ER or other cargoes.

STAR★METHODS

Detailed methods are provided in the online version of this paper and include the following:

- KEY RESOURCES TABLE
- RESOURCE AVAILABILITY
 - Lead contact
 - Materials availability
 - Data and code availability
- EXPERIMENTAL MODEL AND STUDY PARTICIPANT DETAILS
- METHOD DETAILS
 - Molecular cloning
 - Real-time quantitative reverse transcription PCR
 - Co-immunoprecipitation
 - In vitro protein affinity assay
 - Western blot
 - Bimolecular fluorescence complementation
 - Transmission electron microscopy
 - Confocal imaging
 - Protein structure simulation
- QUANTIFICATION AND STATISTICAL ANALYSIS

SUPPLEMENTAL INFORMATION

Supplemental information can be found online at <https://doi.org/10.1016/j.devcel.2023.11.006>.

ACKNOWLEDGMENTS

We thank the Cell Imaging and Analysis Network and the Advanced Bio-Imaging Facility at McGill University for the confocal equipment used and Drs. H. Yu, Y. Guo, and X. Zhao at the Analysis and Testing Center of SKLMT (State Key Laboratory of Microbial Technology, Shandong University) for assistance in laser scanning confocal microscopy. We also thank Dr. W. Zhao from the Harbin Institute of Technology for the kind assistance in the Sparse-deconvolution analysis. J.S. acknowledges grant support from the National Natural Science Foundation of China (no. 32200287), a Qilu Scholarship from Shandong University (Qingdao, China), and financial support from the Key Laboratory of Plant Development and Environmental Adaptation Biology, Ministry of Education, School of Life Sciences, Shandong University. The project was supported by a discovery grant from NSERC, Canada (no. 315863) to H.Z.

AUTHOR CONTRIBUTIONS

J.S. and Y.S. performed most of the experiments and analyzed the data. S.W. created the plasmids for *in vitro* pull-down. X.L. and S.F. performed carbon starvation treatments. C.L. performed the TEM experiment. W.W. and P.L.

performed initial cloning of RABC1 and subcellular localization experiments. J.S. and H.Z. designed and supervised the project and wrote the article with the contributions of other authors.

DECLARATION OF INTERESTS

The authors declare no competing interests.

INCLUSION AND DIVERSITY

One or more of the authors of this paper self-identifies as an underrepresented ethnic minority in their field of research or within their geographical location.

Received: January 4, 2023

Revised: July 30, 2023

Accepted: November 10, 2023

Published: December 5, 2023

REFERENCES

1. Nielsen, E. (2020). The small GTPase superfamily in plants: a conserved regulatory module with novel functions. *Annu. Rev. Plant Biol.* **71**, 247–272.
2. Stenmark, H. (2009). Rab GTPases as coordinators of vesicle traffic. *Nat. Rev. Mol. Cell Biol.* **10**, 513–525.
3. Rutherford, S., and Moore, I. (2002). The Arabidopsis Rab GTPase family: another enigma variation. *Curr. Opin. Plant Biol.* **5**, 518–528.
4. Mayers, J.R., Hu, T., Wang, C., Cárdenas, J.J., Tan, Y., Pan, J., and Bednarek, S.Y. (2017). SCD1 and SCD2 form a complex that functions with the exocyst and RabE1 in exocytosis and cytokinesis. *Plant Cell* **29**, 2610–2625.
5. Zeng, Y., Li, B., Ji, C., Feng, L., Niu, F., Deng, C., Chen, S., Lin, Y., Cheung, K.C.P., Shen, J., et al. (2021). A unique AtSar1D-AtRabD2a nexus modulates autophagosome biogenesis in *Arabidopsis thaliana*. *Proc. Natl. Acad. Sci. USA* **118**, e2021293118.
6. Helen, Y., Leaf, D.S., and Moore, H.H. (1993). Gene cloning and characterization of a GTP-binding Rab protein from mouse pituitary AtT-20 cells. *Gene* **132**, 273–278.
7. Dejgaard, S.Y., and Presley, J.F. (2019). Rab18: new insights into the function of an essential protein. *Cell. Mol. Life Sci.* **76**, 1935–1945.
8. Lütcke, A., Parton, R.G., Murphy, C., Olkkonen, V.M., Dupree, P., Valencia, A., Simons, K., and Zerial, M. (1994). Cloning and subcellular localization of novel rab proteins reveals polarized and cell type-specific expression. *J. Cell Sci.* **107**, 3437–3448.
9. Dejgaard, S.Y., Murshid, A., Erman, A., Kizilay, O., Verbich, D., Lodge, R., Dejgaard, K., Ly-Hartig, T.B., Pepperkok, R., Simpson, J.C., et al. (2008). Rab18 and Rab43 have key roles in ER-Golgi trafficking. *J. Cell Sci.* **121**, 2768–2781.
10. Gerondopoulos, A., Bastos, R.N., Yoshimura, S., Anderson, R., Carpanini, S., Alianian, I., Handley, M.T., and Barr, F.A. (2014). Rab18 and a Rab18 GEF complex are required for normal ER structure. *J. Cell Biol.* **205**, 707–720.
11. Xu, D.J., Li, Y.Q., Wu, L.Z., Li, Y., Zhao, D.Y., Yu, J.H., Huang, T.Z., Ferguson, C., Parton, R.G., Yang, H.Y., et al. (2018). Rab18 promotes lipid droplet (LD) growth by tethering the ER to LDs through SNARE and NRZ interactions. *J. Cell Biol.* **217**, 975–995.
12. Takáts, S., Lévay, L., Boda, A., Tóth, S., Simon-Vecsei, Z., Rubics, A., Varga, Á., Lippai, M., Lőrincz, P., Glatz, G., et al. (2021). The Warburg Micro Syndrome-associated Rab3GAP-Rab18 module promotes autolysosome maturation through the Vps34 complex I. *FEBS Journal* **288**, 190–211.
13. Stolz, A., Ernst, A., and Dikic, I. (2014). Cargo recognition and trafficking in selective autophagy. *Nat. Cell Biol.* **16**, 495–501.
14. Chino, H., and Mizushima, N. (2020). ER-phagy: quality control and turnover of endoplasmic reticulum. *Trends Cell Biol.* **30**, 384–398.

15. Molinari, M. (2021). ER-phagy responses in yeast, plants, and mammalian cells and their crosstalk with UPR and ERAD. *Dev. Cell* 56, 949–966.
16. Brandizzi, F. (2021). Maintaining the structural and functional homeostasis of the plant endoplasmic reticulum. *Dev. Cell* 56, 919–932.
17. Hu, S., Ye, H., Cui, Y., and Jiang, L. (2020). AtSec62 is critical for plant development and is involved in ER-phagy in *Arabidopsis thaliana*. *J. Integr. Plant Biol.* 62, 181–200.
18. Wu, J., Michaeli, S., Picchianti, L., Dagdas, Y., Galili, G., and Peled-Zehavi, H. (2021). AT1 (ATG8-interacting protein 1) and AT12 define a plant starvation-induced reticulophagy pathway and serve as MSBP1/MAPR5 cargo receptors. *Autophagy* 17, 3375–3388.
19. Chang, C., Jensen, L.E., and Hurley, J.H. (2021). Autophagosome biogenesis comes out of the black box. *Nat. Cell Biol.* 23, 450–456.
20. Melia, T.J., Lystad, A.H., and Simonsen, A. (2020). Autophagosome biogenesis: from membrane growth to closure. *J. Cell Biol.* 219.
21. Mizushima, N. (2018). A brief history of autophagy from cell biology to physiology and disease. *Nat. Cell Biol.* 20, 521–527.
22. Marshall, R.S., and Vierstra, R.D. (2018). Autophagy: the master of bulk and selective recycling. *Annu. Rev. Plant Biol.* 69, 173–208.
23. Shpilka, T., Weidberg, H., Pietrovski, S., and Elazar, Z. (2011). Atg8: an autophagy-related ubiquitin-like protein family. *Genome Biol.* 12, 226.
24. Marshall, R.S., Hua, Z., Mali, S., McLoughlin, F., and Vierstra, R.D. (2019). ATG8-binding UIM proteins define a new class of autophagy adaptors and receptors. *Cell* 177, 766–781.e24.
25. Schütter, M., Giavalisco, P., Brodesser, S., and Graef, M. (2020). Local fatty acid channeling into phospholipid synthesis drives phagophore expansion during autophagy. *Cell* 180, 135–149.e14.
26. Kotani, T., Kirisako, H., Koizumi, M., Ohsumi, Y., and Nakatogawa, H. (2018). The Atg2-Atg18 complex tethers pre-autophagosomal membranes to the endoplasmic reticulum for autophagosome formation. *Proc. Natl. Acad. Sci. USA* 115, 10363–10368.
27. Xiong, Y., Contento, A.L., and Bassham, D.C. (2005). AtATG18a is required for the formation of autophagosomes during nutrient stress and senescence in *Arabidopsis thaliana*. *Plant J.* 42, 535–546.
28. Xiong, Y., Contento, A.L., Nguyen, P.Q., and Bassham, D.C. (2007). Degradation of oxidized proteins by autophagy during oxidative stress in *Arabidopsis*. *Plant Physiol.* 143, 291–299.
29. Liu, Y.M., Xiong, Y., and Bassham, D.C. (2009). Autophagy is required for tolerance of drought and salt stress in plants. *Autophagy* 5, 954–963.
30. Liu, Y., Burgos, J.S., Deng, Y., Srivastava, R., Howell, S.H., and Bassham, D.C. (2012). Degradation of the endoplasmic reticulum by autophagy during endoplasmic reticulum stress in *Arabidopsis*. *Plant Cell* 24, 4635–4651.
31. Aroca, A., Yruela, I., Gotor, C., and Bassham, D.C. (2021). Persulfidation of ATG18a regulates autophagy under ER stress in *Arabidopsis*. *Proc. Natl. Acad. Sci. USA* 118, e2023604118.
32. Ge, S., Zhang, R.X., Wang, Y.F., Sun, P., Chu, J., Li, J., Sun, P., Wang, J., Hetherington, A.M., and Liang, Y.K. (2022). The *Arabidopsis* Rab protein RABC1 affects stomatal development by regulating lipid droplet dynamics. *Plant Cell* 34, 4274–4292.
33. Schmid, M., Davison, T.S., Henz, S.R., Pape, U.J., Demar, M., Vingron, M., Schölkopf, B., Weigel, D., and Lohmann, J.U. (2005). A gene expression map of *Arabidopsis thaliana* development. *Nat. Genet.* 37, 501–506.
34. Zheng, H., Camacho, L., Wee, E., Batoko, H., Legen, J., Leaver, C.J., Malhó, R., Hussey, P.J., and Moore, I. (2005). A Rab-E GTPase mutant acts downstream of the Rab-D subclass in biosynthetic membrane traffic to the plasma membrane in tobacco leaf epidermis. *Plant Cell* 17, 2020–2036.
35. Sun, J., Wang, W., and Zheng, H. (2022). ROOT HAIR DEFECTIVE3 is a receptor for selective autophagy of the endoplasmic reticulum in *Arabidopsis*. *Front. Plant Sci.* 13, 817251.
36. Stefano, G., and Brandizzi, F. (2014). Unique and conserved features of the plant ER-shaping GTPase RHD3. *Cell. Logist.* 4, e28217.
37. Sun, J., Zhang, M., Qi, X., Doyle, C., and Zheng, H. (2020). Armadillo-repeat kinesin1 interacts with *Arabidopsis* atlastin RHD3 to move ER with plus-end of microtubules. *Nat. Commun.* 11, 5510.
38. Li, C., Duckney, P., Zhang, T., Fu, Y., Li, X., Kroon, J., De Jaeger, G., Cheng, Y., Hussey, P.J., and Wang, P. (2022). TraB family proteins are components of ER-mitochondrial contact sites and regulate ER-mitochondrial interactions and mitophagy. *Nat. Commun.* 13, 5658.
39. Lai, Y.S., Stefano, G., Zemelis-Durfee, S., Ruberti, C., Gibbons, L., and Brandizzi, F. (2018). Systemic signaling contributes to the unfolded protein response of the plant endoplasmic reticulum. *Nat. Commun.* 9, 3918.
40. Polson, H.E., de Lartigue, J., Riggan, D.J., Reedijk, M., Urbé, S., Clague, M.J., and Tooze, S.A. (2010). Mammalian Atg18 (WIPI2) localizes to omega-glycoside-anchored phagophores and positively regulates LC3 lipidation. *Autophagy* 6, 506–522.
41. Singh, R., Kaushik, S., Wang, Y., Xiang, Y., Novak, I., Komatsu, M., Tanaka, K., Cuervo, A.M., and Czaja, M.J. (2009). Autophagy regulates lipid metabolism. *Nature* 458, 1131–1135.
42. Bassham, D.C., Laporte, M., Marty, F., Moriyasu, Y., Ohsumi, Y., Olsen, L.J., and Yoshimoto, K. (2006). Autophagy in development and stress responses of plants. *Autophagy* 2, 2–11.
43. He, Y., Gao, J., Luo, M., Gao, C., Lin, Y., Wong, H.Y., Cui, Y., Zhuang, X., and Jiang, L. (2023). VAMP724 and VAMP726 are involved in autophagosome formation in *Arabidopsis thaliana*. *Autophagy* 19, 1406–1423.
44. Zhuang, X., Chung, K.P., Cui, Y., Lin, W., Gao, C., Kang, B.H., and Jiang, L. (2017). ATG9 regulates autophagosome progression from the endoplasmic reticulum in *Arabidopsis*. *Proc. Natl. Acad. Sci. USA* 114, E426–E435.
45. Ye, H., Gao, J., Liang, Z., Lin, Y., Yu, Q., Huang, S., and Jiang, L. (2022). *Arabidopsis* ORP2A mediates ER-autophagosomal membrane contact sites and regulates PI3P in plant autophagy. *Proc. Natl. Acad. Sci. USA* 119, e2205314119.
46. Pu, Y., Luo, X., and Bassham, D.C. (2017). TOR-dependent and -independent pathways regulate autophagy in *Arabidopsis thaliana*. *Front. Plant Sci.* 8, 1204.
47. Liu, Y., and Bassham, D.C. (2010). TOR is a negative regulator of autophagy in *Arabidopsis thaliana*. *PLoS One* 5, e11883.
48. Stephani, M., Picchianti, L., and Dagdas, Y. (2021). C53 is a cross-kingdom conserved reticulophagy receptor that bridges the gap between-selective autophagy and ribosome stalling at the endoplasmic reticulum. *Autophagy* 17, 586–587.
49. Zhao, Y.G., Liu, N., Miao, G., Chen, Y., Zhao, H., and Zhang, H. (2018). The ER contact proteins VAPA/B interact with multiple autophagy proteins to modulate autophagosome biogenesis. *Curr. Biol.* 28, 1234–1245.e4.
50. Thompson, A.R., Doelling, J.H., Suttangkakul, A., and Vierstra, R.D. (2005). Autophagic nutrient recycling in *Arabidopsis* directed by the ATG8 and ATG12 conjugation pathways. *Plant Physiol.* 138, 2097–2110.
51. Sun, J., and Zheng, H. (2018). Efficient ER fusion requires a dimerization and a C-terminal tail mediated membrane anchoring of RHD3. *Plant Physiol.* 176, 406–417.
52. Schindelin, J., Arganda-Carreras, I., Frise, E., Kaynig, V., Longair, M., Pietzsch, T., Preibisch, S., Rueden, C., Saalfeld, S., Schmid, B., et al. (2012). Fiji: an open-source platform for biological-image analysis. *Nat. Methods* 9, 676–682.
53. Zhao, W., Zhao, S., Li, L., Huang, X., Xing, S., Zhang, Y., Qiu, G., Han, Z., Shang, Y., Sun, D.E., et al. (2022). Sparse deconvolution improves the resolution of live-cell super-resolution fluorescence microscopy. *Nat. Biotechnol.* 40, 606–617.
54. Sun, J., Movahed, N., and Zheng, H. (2020). LUNAPARK is an E3 ligase that mediates degradation of ROOT HAIR DEFECTIVE3 to maintain a tubular ER network in *Arabidopsis*. *Plant Cell* 32, 2964–2978.

STAR★METHODS

KEY RESOURCES TABLE

REAGENT or RESOURCE	SOURCE	IDENTIFIER
Antibodies		
Mouse monoclonal anti-GFP	Abclonal	Cat#: AE012; RRID: AB_2770402
Mouse polyclonal anti-mCherry	ELK Biotechnology	Cat#: EA012
Mouse monoclonal anti-His	Transgen Biotech	Cat#: HT501, RRID:AB_2801417
Mouse monoclonal anti-GST	Transgen Biotech	Cat#: HT601, RRID:AB_2922384
Mouse monoclonal anti-HA	Proteintech	Cat#: 66006-2-Ig, RRID:AB_2881490
Rabbit polyclonal anti-BiP2	PhytoAB	Cat#: PHY1481A
Rabbit polyclonal anti-PEX12	PhytoAB	Cat#: PHY7126S
Rabbit polyclonal anti-CYC1	PhytoAB	Cat#: PHY0566A
GFP-Trap MA	ChromoTek	Cat#: gtma-20; RRID: AB_2631358
Anti-mcherry Nanobody Magarose Beads	AlpaLifeBio	Cat#: KTS1337
Glutathione Magarose Beads	Smart-Lifesciences	Cat#: SM002005
Ni NTA Magarose Beads	Smart-Lifesciences	Cat#: SM008005
Chemicals, peptides, and recombinant proteins		
Protease inhibitor cocktail	Sigma-Aldrich	Cat#:P9599
IGEPAL CA-630	Sigma-Aldrich	Cat#:I8896
Concanamycin A	Sigma-Aldrich	Cat#:C9705
E64d	Sigma-Aldrich	Cat#:E8940
Dithiothreitol	Coolaber	Cat#:CD4941-5g
AZD8055	Meilunbio	Cat#:1009298-09-2
Tunicamycin	Cell Signaling Technology	Cat#:12819
Critical commercial assays		
FastPure Universal Plant Total RNA Isolation Kit	Vazyme	Cat#:RC411-01
HiScript®III 1st Strand cDNA Synthesis Kit	Vazyme	Cat#: R312-01
Experimental models: Organisms/strains		
Arabidopsis thaliana: WT Col.0	ABRC	N/A
Arabidopsis thaliana: <i>rabc1</i> (SALK_012129)	Ge et al. ³²	N/A
Arabidopsis thaliana: <i>atg5-1</i>	Thompson et al. ⁵⁰	N/A
Arabidopsis thaliana: 35S::YFP-RABC1 <i>rabc1</i>	This paper	N/A
Arabidopsis thaliana: 35S::YFP-RABC1 mCherryHDEL <i>rabc1</i>	This paper	N/A
Arabidopsis thaliana: 35S::YFP-RABC1 mCherry-ATG8e <i>rabc1</i>	This paper	N/A
Arabidopsis thaliana: 35S::YFP-RABC1 mCherry-ATG18a <i>rabc1</i>	This paper	N/A
Arabidopsis thaliana: pRABC1::YFP-RABC1 <i>rabc1</i>	This paper	N/A
Arabidopsis thaliana: pRABC1::YFP-RABC1 ST-RFP <i>rabc1</i>	This paper	N/A
Arabidopsis thaliana: pRABC1::mNeonGreen-RABC1 <i>rabc1</i>	This paper	N/A
Arabidopsis thaliana: pRABC1::mNeonGreen-RABC1 mCherry-ATG18a <i>rabc1</i>	This paper	N/A
Arabidopsis thaliana: 35S::YFP-RABC1	This paper	N/A
Arabidopsis thaliana: 35S::YFP-RABC1 <i>atg5-1</i>	This paper	N/A

(Continued on next page)

Continued

REAGENT or RESOURCE	SOURCE	IDENTIFIER
Arabidopsis thaliana: YFP-TMC	Sun et al. ³⁵	N/A
Arabidopsis thaliana: YFP-TMC <i>rabc1</i>	This paper	N/A
Arabidopsis thaliana: pUBQ10::mNeonGreen-ATG18a	This paper	N/A
Arabidopsis thaliana: pUBQ10::mNeonGreen-ATG18a <i>rabc1</i>	This paper	N/A
Arabidopsis thaliana: pUBQ10::mNeonGreen-ATG18a mScarletHDEL	This paper	N/A
Arabidopsis thaliana: pUBQ10::mNeonGreen-ATG18a mScarletHDEL <i>rabc1</i>	This paper	N/A
Oligonucleotides		
RABC1 forward primer: ATGGGTTCTTCGTC AGGACAACC	This paper	N/A
RABC1 reverse primer: CTAAGACGAGCAG CAGTAGC	This paper	N/A
RABC1 qRT forward primer: AGGACGCTAA CAAGTTCGT	This paper	N/A
RABC1 qRT reverse primer: TCCCGACAAG CATCTTAATGC	This paper	N/A
RABC1(S27N) forward primer: GTTGGAAAGA ACTCTTTGTTGAGTTTC	This paper	N/A
RABC1(S27N) reverse primer: CAAAAGAGAGT TCTTCCAACACCAGAACATC	This paper	N/A
RABC1(Q71L) forward primer: GATACAGCTGG GCTAGAGAGATTAG	This paper	N/A
RABC1(Q71L) reverse primer: CTCTCTAGCC CAGCTGTATCCC	This paper	N/A
ATG18a forward primer: ATGCCACCGTATC TTCTTCCTC	This paper	N/A
ATG18a reverse primer: TTAGAAAATGAAGG CGGTTTCAGACAG	This paper	N/A
Recombinant DNA		
35S::YFP-RABC1	This paper	N/A
35S::YFP-RABC1(S27N)	This paper	N/A
35S::YFP-RABC1(Q71L)	This paper	N/A
35S::YFP	This paper	N/A
pRABC1::YFP-RABC1	This paper	N/A
pRABC1::mNeonGreen-RABC1	This paper	N/A
mCherry-HDEL	Sun and Zheng ⁵¹	N/A
mCherry-ATG5	This paper	N/A
mCherry-ATG8e	This paper	N/A
mCherry-ATG18a	This paper	N/A
ST-RFP	Sun and Zheng ⁵¹	N/A
Mito-mCherry	This paper	N/A
PX-mCherry	This paper	N/A
Sec-mCherry	This paper	N/A
GST	This paper	N/A
GST-RABC1	This paper	N/A
GST-RABC1(S27N)	This paper	N/A
GST-RABC1(Q71L)	This paper	N/A
His-ATG18a	This paper	N/A
HA-RABC1	This paper	N/A

(Continued on next page)

Continued

REAGENT or RESOURCE	SOURCE	IDENTIFIER
HA-RABC1(S27N)	This paper	N/A
HA-RABC1(Q71L)	This paper	N/A
YFP-TMC	Sun et al. ³⁵	N/A
mCherry-TMC	This paper	N/A
Software and algorithms		
Image J	Schindelin et al. ⁵²	https://imagej.nih.gov/ij/
Sparse-deconvolution	Zhao et al. ⁵³	https://github.com/WeisongZhao/Sparse-SIM/releases/tag/v1.0.3

RESOURCE AVAILABILITY

Lead contact

Further information and requests for reagents may be directed to and will be fulfilled by the Lead Contact, Huanquan Zheng (hugo.zheng@mcgill.ca).

Materials availability

All data required to support the claims of this paper are included in the main and [supplemental information](#).

This paper does not report original code.

All reagents generated in this study are available on request from the [lead contact](#).

Data and code availability

All data required to substantiate the claims of this paper are included in main or [supplemental information](#).

This paper does not report original code.

Any additional information required to reanalyze the data reported in this paper is available from the [lead contact](#) upon request.

EXPERIMENTAL MODEL AND STUDY PARTICIPANT DETAILS

Arabidopsis ecotype Columbia-0 (Col-0) was the genetic background for all mutants and transgenic lines. The *rabc1* mutant (SALK_012129) was ordered from the Arabidopsis Biological Resource Center. PCR and RT-PCR were performed to identify the homozygous mutant line. 35Spro::YFP-RABC1, RABC1pro::YFP-RABC1 and RABC1pro::mNeonGreen-RABC1 were transformed into the *rabc1* mutant to generate 35Spro::YFP-RABC1 *rabc1*, RABC1pro::YFP-RABC1 *rabc1* and RABC1pro::mNeonGreen-RABC1 *rabc1* transgenic plants. UBIQ10pro::mNeonGreen-ATG18a was transformed into wild type and the *rabc1* mutant, respectively. Subsequently, mScarletHDEL was transformed into UBIQ10pro::mNeonGreen-ATG18a WT and UBIQ10pro::mNeonGreen-ATG18a *rabc1*, respectively to generate mScarletHDEL expressed lines.

All plants were grown on 1/2 Murashige Skoog (MS) medium with 1% sucrose or in the soil under 16 h in light and 8 h in dark with 60% humidity at 22°C. For the carbon starvation treatment, wild type and *rabc1* seedlings were germinated and grown on 1/2 MS medium without sucrose, or 5-day-old seedlings grown on 1/2 MS medium supplied with 1% sucrose was moved to 1/2 MS medium without sucrose and grown in the dark for 10 days, then recovered under 16 h light for 7 days. For the ER stress treatment, wild type and *rabc1* seeds were directly sown on the 1/2 MS medium with 1mM dithiothreitol (DTT). To induce acute stress in plants, 5-day-old seedlings were subjected to different treatments. Specifically, the seedlings were transferred into 1/2 MS liquid medium containing 2mM DTT or 5µg/ml TM along with 1% sucrose to induce ER stress. For carbon starvation-induced stress, the seedlings were placed in 1/2 MS liquid medium without sucrose and kept in the dark. To induce nitrogen starvation, the seedlings were placed in 1/2 MS liquid medium without a nitrogen supply but with 1% sucrose. Additionally, to examine the effect of TOR signaling on stress response, the seedlings were treated with 1µM AZD8055 in 1/2 MS liquid medium supplemented with 1% sucrose. These stress treatments were applied for various durations. For visualization of YFP-RABC1 and mCherryHDEL in the vacuole, 0.1µM Concanavalin A (ConcA) was added in 1/2 MS medium. For transient expression experiments involving E64d treatment, *N. benthamiana* leaves were infiltrated with 400µM E64d at the same locations 36 h after filtration (12 h prior to imaging).

METHOD DETAILS

Molecular cloning

To generate YFP-RABC1, mCherry-ATG18a, mCherry-ATG5, mNeonGreen-RABC1, mNeonGreen-ATG18a and HA-RABC1, the coding sequence of RABC1, ATG18a and ATG5 were cloned into the pGEM-Gate entry vector, and then subcloned into pEarleyGate 104, pEarleyGate 104-mCherry, pEarleyGate 104-mNeonGreen and pEarleyGate 201 via the gateway reaction. To generate YFP-RABC1(S27N), YFP-RABC1(Q71L), HA-RABC1(S27N) and HA-RABC1(Q71L), overlap PCR was performed on pGEM-RABC1 to

create pGEM-RABC1(S27N) and pGEM-RABC1, then subcloned into pEarleyGate 104 and pEarleyGate 201 through the gateway reaction. The 35S promoter of pEarleyGate 104-mNeonGreen was replaced by the UBQ10 promoter or the RABC1 promoter (836bp upstream of ATG) through ClonExpress II system (Vazyme) to generate UBQpro::mNeonGreen-ATG18a, RABC1pro::YFP-RABC1 and RABC1pro::mNeonGreen-RABC1.

Real-time quantitative reverse transcription PCR

Following carbon starvation for various durations, total RNAs were extracted from the seedlings using the FastPure Universal Plant Total RNA Isolation Kit (Vazyme, RC411-01). Subsequently, single-strand cDNA was synthesized using the HiScript®III 1st Strand cDNA Synthesis Kit (Vazyme, R312-01). The expression levels of RABC1 were assessed utilizing RABC1 primers ([key resources table](#)), while Actin2 was employed as the internal control. Real-time qRT-PCR reactions were conducted in three technical replicates using LineGene 4800 (BIOER).

Co-immunoprecipitation

N. benthamiana leaves infiltrated with different combinations of proteins described or stress treated *Arabidopsis* seedlings were ground to powder in liquid nitrogen and extracted with the extraction buffer (50 mM Tris-HCl, pH 7.5, 150 mM NaCl, 10% [v/v] glycerol, 0.5% [v/v] IGEPAL CA-630, and 1% [v/v] of Protease Inhibitor Cocktail. The extraction was centrifuged at 17,000g for 10 mins at 4°C. Then the supernatant was collected and mixed with 25 µl GFP-Trap_MA beads or Anti-mcherry Nanobody Magarose Beads for 1 h at 4°C. The beads were magnetically separated and washed three times with wash buffer (10mM Tris-HCl, pH 7.5, and 150mM NaCl). Next, the beads were resuspended in 100 µl 2x SDS-loading buffer and boiled for 10 mins for western blot.

In vitro protein affinity assay

To generate GST-RABC1, GST-RABC1(S27N) and GST-RABC1(Q71L), the fragments of RABC1, RABC1(S27N) and RABC1(Q71L) were cloned into the pGEX-4T-1 vector through the T4 ligation. To generate His-ATG18a, the ATG18a fragment was cloned into the pET28a vector through the T4 ligation. All the constructs were transformed into TSsetta (DE3) cells (Tsingke Biotechnology). The cells were cultured in LB medium for overnight. Then the OD was adjusted to 0.1 and cultured for another 2 h (OD = 0.4-0.6). 0.5 µM IPTG was added into the solution and cultured for 4 h. Then the bacteria cells were collected by centrifuging and resuspended in the extraction buffer (140mM NaCl, 2.7mM KCl, 10 mM Na₂HPO₄, 1.8 mM KH₂PO₄, pH 7.4, and 1%[v/v] of Protease Inhibitor Cocktail [[catalog no. P9599; Sigma-Aldrich](#)]). Then proteins were extracted with sonication. His-ATG18a extracts were mixed with different GST extracts, and incubated with GST beads (Smart-Lifesciences Biotechnology) on the rotator for 4 h at 4°C. Next, GST beads were washed three times with extraction buffer and boiled in 100 µl 2x SDS-loading buffer for western blot.

Western blot

Protein samples were loaded on 10% SDS-PAGE gel. Mouse anti-GFP antibody (AE012, Abclonal, 1:5000 dilution), mouse anti-mCherry antibody (EA012, ELK Biotechnology, 1:5000 dilution), mouse anti-His antibody (HT501, TransGen, 1:5000), mouse anti-GST antibody (HT601, TransGen, 1:5000), rabbit anti-BiP2 antibody (PHY1481A, Phytoab, 1:5000), rabbit anti-PEX12 antibody (PHY7126S, Phytoab, 1:5000) and rabbit anti-CYC1 antibody (PHY0566A, Phytoab, 1:5000) were used for western blot. The secondary goat anti-mouse IgG (SA002, ELK Biotechnology, 1:10000) and goat anti-rabbit IgG (AS09 602, Agrisera, 1:10000) were used.

Bimolecular fluorescence complementation

RABC1, RABC1 (S27N), RABC1 (Q71L) were cloned into 3-in-1 BiFC vector.⁵⁴ mCherryHDEL in the same expression cassette was used as the expression control for proteins to be tested. The transient expression of proteins in *N. benthamiana* leaves was done with OD = 0.01.

Transmission electron microscopy

TEM was performed as previously described.³⁸ Using the 0.5 cm root segments as samples, which were collected from the seedlings after -C treatment 6h. All samples were prefixed in 2.5 % glutaraldehyde (v/v in 0.1 M phosphate buffer, pH 7.2) for 2 h, and then rinsed 3 times with 0.1 M phosphate buffer (pH 7.2). They were post-fixed in 1 % OsO₄ for 2 h, followed by three 15 min rinses with phosphate buffer. Afterwards, the samples were dehydrated through an acetone series (30 %, 50 %, 70 %, 90 %, 100 %, 100 %, 100 %) (v/v in dd H₂O) at room temperature, samples were incubated for 10-15 min at each concentration. Then the samples were infiltrated in a graded scale of 3:1, 1:1, 1:3 (v/v) acetone/SPI-PON 812 resin and, as the last step, in 100 % (v/v) SPI-PON 812 resin (SPI Supplies, West Chester), for 12 h per step. Samples were embedded in SPI-PON 812 resin and polymerized at 60 °C for 48 h. Ultrathin sections (80 nm) were prepared using an EM UC7 Ultracut ultramicrotome (Leica, UC7). Sections were observed and photographed using a transmission electron microscope (Hitachi H-7650) at an accelerating voltage of 80.0 kV.

Confocal imaging

Confocal imaging was done with a Leica SP8 point-scanning confocal system on a Leica DMI6000B inverted microscope equipped with spectral fluorescent light detectors (three photomultiplier tubes, one hybrid high sensitivity detector). A 63/1.4 oil objective was used for all imaging. A 488nm laser was used to excite YFP/mNeonGreen, and a 552 nm laser was used to excite RFP/mCherry/mScarlet. Two channels were excited sequentially. Emission filters were set as 490 to 560 nm for YFP and as 580 to 660 nm for

RFP/mCherry-BiFC images were taken by LSM 900 with 63/1.4 oil DIC M27 objective. 488nm and 561nm were used to excite mCherryHDEL and BiFC signal, respectively. Emission filters were set as 410nm to 570nm for BiFC signal and as 580-617 nm for mCherryHDEL.

Protein structure simulation

RABC1 and ATG18a structures were generated by AlphaFold2 (<https://alphafold.ebi.ac.uk/>) and ATG18a was used as the ligand. The molecular docking required the preparation of ligands and proteins using the PyMOL software. For the target protein, its crystal structure was preprocessed, including the removal of water molecules and addition of hydrogen atoms. The Affinity value (in kcal/mol) represents the binding strength between the ligand and the protein (-340.6). Molecular docking was performed using Hex 8.0.0 (<https://hex.loria.fr/>), where a lower affinity indicates a more stable binding between the ligand and the receptor. Finally, the docking results were analyzed and observed using the PyMOL software.

QUANTIFICATION AND STATISTICAL ANALYSIS

All images were processed and analyzed with Image J (Fiji). Deconvolution of live images were performed with Sparse-deconvolution.⁵³ For the quantification of RABC1 or ATG18a following Concanavalin A (ConcA) treatment, we focused on the central region of plant cells and determined the number of punctae localized within the vacuole. The number and size of ATG18a were quantified using the "Analyze Particles" function in Fiji. To quantify the percentage of BiFC signal or ATG18a punctae on the ER, the number of punctae co-localized with the ER marker was counted and divided by the total punctae number observed in each cell. To quantify the relative ratio between ATG18a punctae and the cytosolic signal, the mean signal intensity of ATG18a punctae ($n > 10$) was determined and compared to the mean intensity of the cytosolic signal (the non-punctate, diffusing signal) to get the relative ratio in each cell. Subsequently, the average ratio was calculated based on the data collected from 20 cells.

Statistical analysis was conducted on data from multiple groups that satisfied the criteria of homogeneity of variance and adherence to a normal distribution. This analysis employed ANOVA followed by Fisher's Least Significant Difference (LSD) test. Each statistical assessment presented in the figures represents one of at least three independent replicates. Pertinent information including the specific statistical test employed, identification of statistically distinct groups or associated p-values, statistical parameters (SEM or SD), sample sizes (n), and the nature of the sample (e.g., leaves or root cells) is comprehensively provided within the figure legends.

Supplemental information

**An Arabidopsis Rab18 GTPase promotes autophagy
by tethering ATG18a to the ER in response
to nutrient starvation**

Jiaqi Sun, Yang Shao, Songyang Wang, Xunzheng Li, Shuqing Feng, Weina Wang, Pierre Leroy, Chengyang Li, and Huanquan Zheng

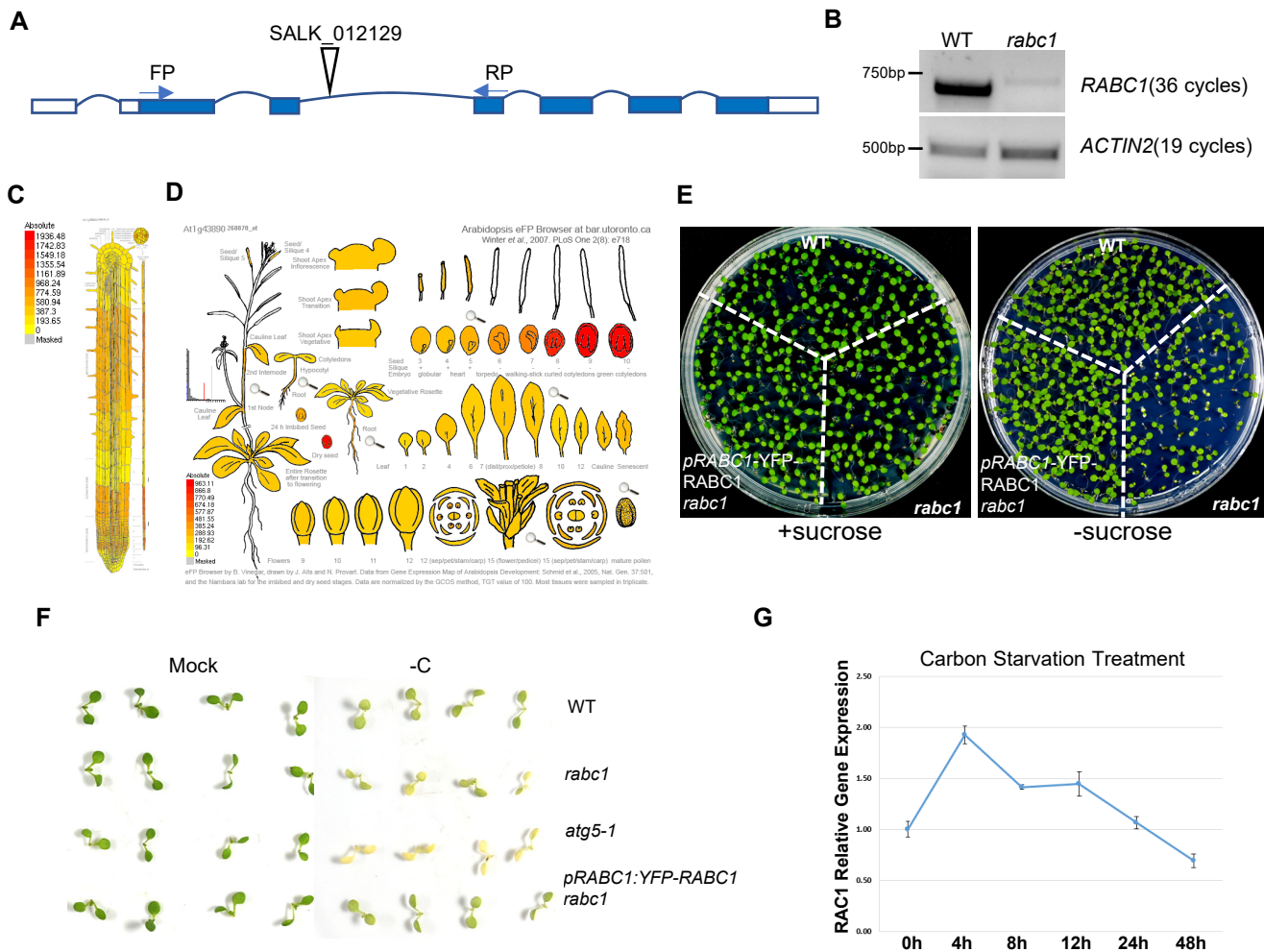


Figure S1. The characterization of *rabc1* and expression of *RABC1*, Related to Figure 1.

(A) The position of the T-DNA insertion in the *rabc1* mutant (SALK_012129) identified. Open boxes indicate un-translational regions, blue boxes indicate exons, blue lines indicate introns.

(B) *rabc1* is a knock down mutant. The FP and RP primers indicated in (A) were used in RT-PCR of *RABC1* (36 cycles). *ACTIN2* (19 cycles) was used as the loading control.

(C-D) The expression of *RABC1* in roots (C) and different tissues (D). The data ³³ was adapted from the Arabidopsis eFP Browser .

(E) Seedlings of wild type (WT), *rabc1* and *pRABC1::YFP-RABC1 rabc1* grown on $\frac{1}{2}$ MS with (the left side) or without (the right side) sucrose for 7 days.

(F) Seedlings of WT, *rabc1*, *atg5-1* and *35S::YFP-RABC1 rabc1* grown on $\frac{1}{2}$ MS without sucrose for 7 days, and moved to $\frac{1}{2}$ MS without sucrose and kept in the dark for 10 days (-C).

(G) The transcription level of *RABC1* after carbon starvation treatment. The gene expression of *RABC1* was investigated using qRT-PCR at various time points (0h, 4h, 8h, 12h, 24h, 48h) subsequent to the carbon starvation treatment.

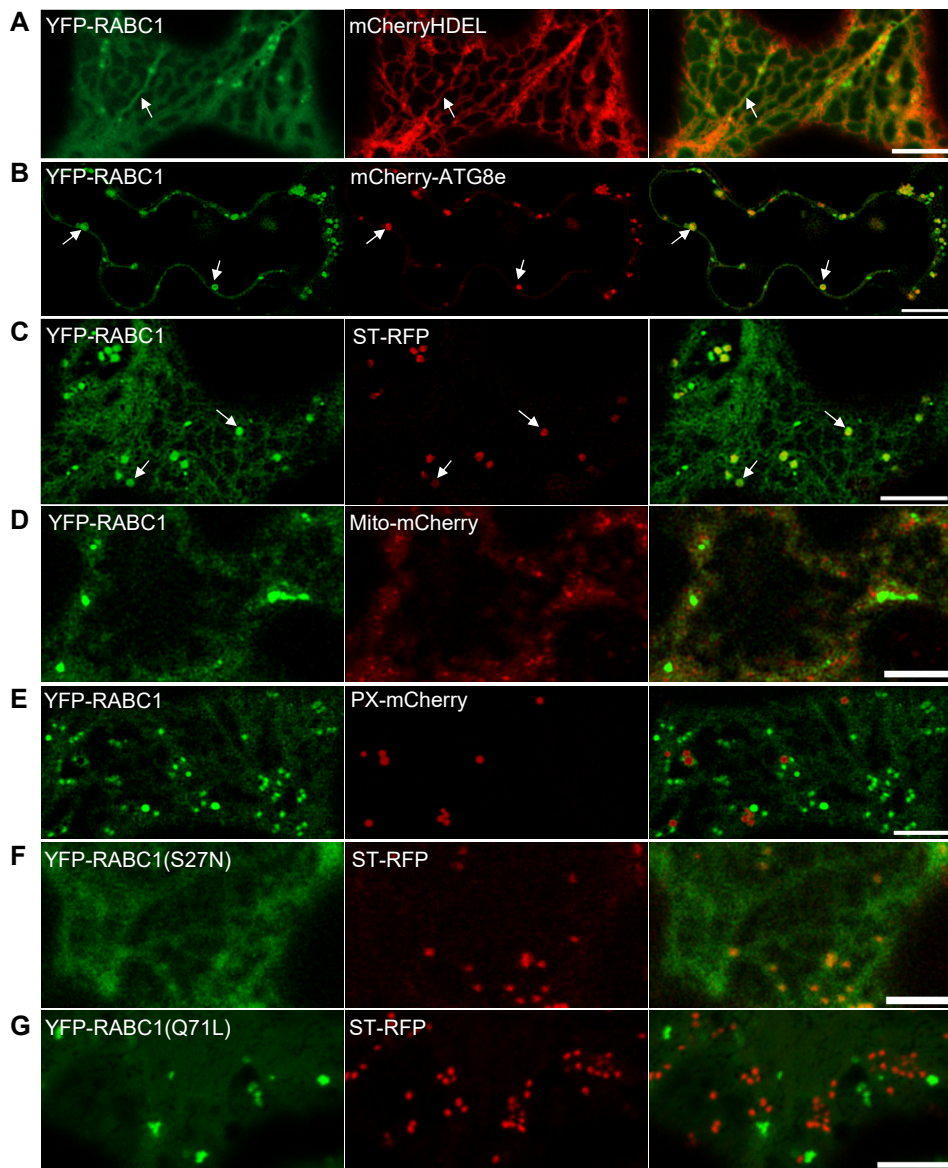


Figure S2. The subcellular localization of RABC1 transiently expressed in *N. benthamiana* leaves, Related to Figure 2.

(A-C) YFP-RABC1 is partially co-localized with the ER labelled by mCherryHDEL (pointed by arrows) (A), with autophagosomes marked by mCherry-ATG8e (pointed by arrows) (B), to Golgi bodies marked by ST-RFP (pointed by arrows) (C) when co-expressed in *N. benthamiana* leaves. Scale bar = 10 μ m.

(D-E) YFP-RABC1 is not co-localized with mitochondria marked by Mito-mCherry (D) and peroxisomes labelled by PX-mCherry (E), when co-expressed in *N. benthamiana* leaves. Scale bar = 10 μ m.

(F-G) Targeting of ST-RFP to Golgi is not affected by either dominant negative form of YFP-RABC1(S27N) (F) or constitutively active form of YFP-RABC1(Q71L) when co-expressed in *N. benthamiana* leaves. Scale bar = 10 μ m.

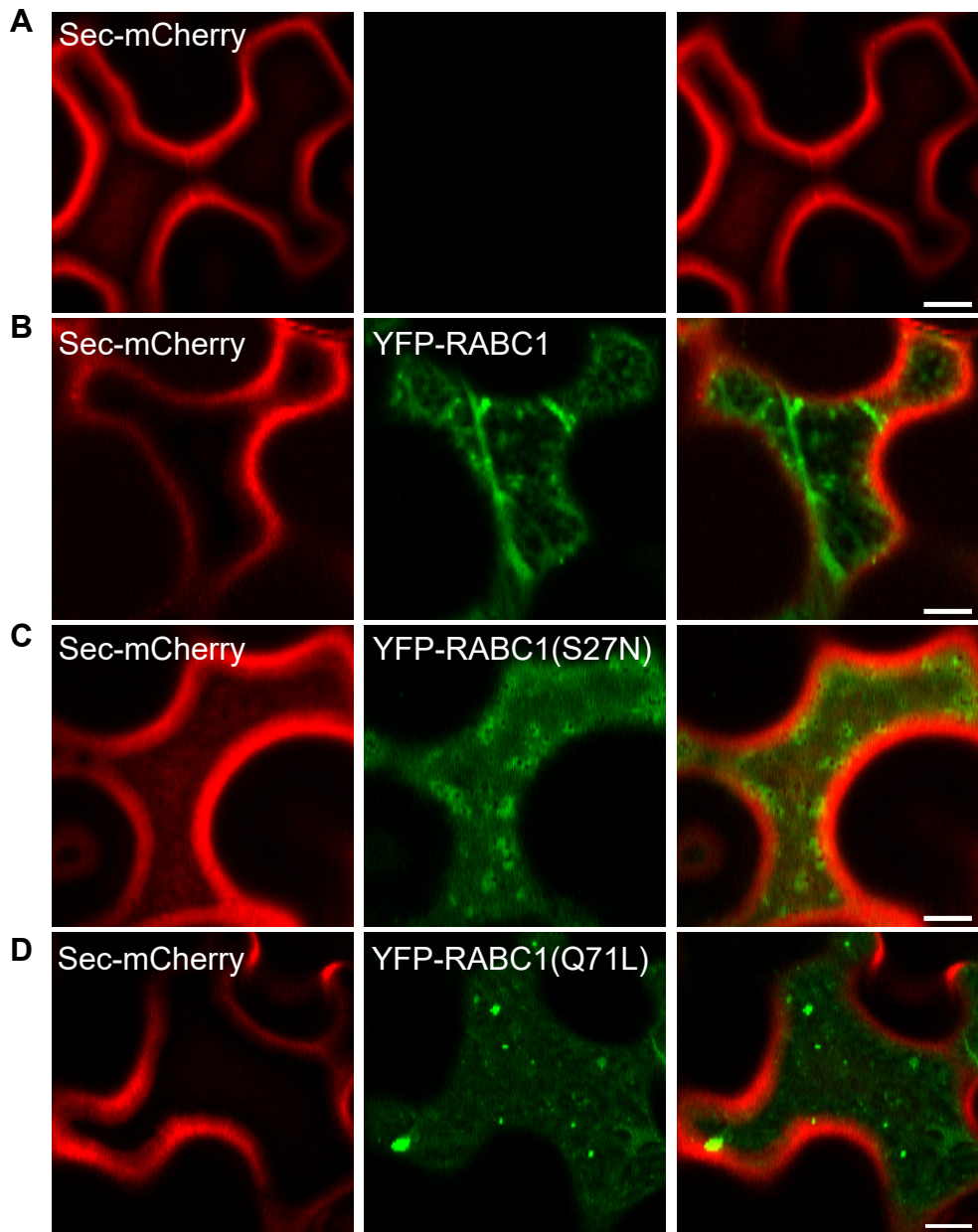


Figure S3. RABC1 does not inhibit secretion of sec-mCherry, Related to Figure 3.
(A-D) Confocal images of Sec-mCherry expressed alone (A) or co-expressed with YFP-RABC1 (B), YFP-RABC1 (S27N) (C), and YFP-RABC1 (Q71L) (D). None of the RABC1 variants had significant impact on secretion of Sec-mCherry. Scale bar = 10 μ m.

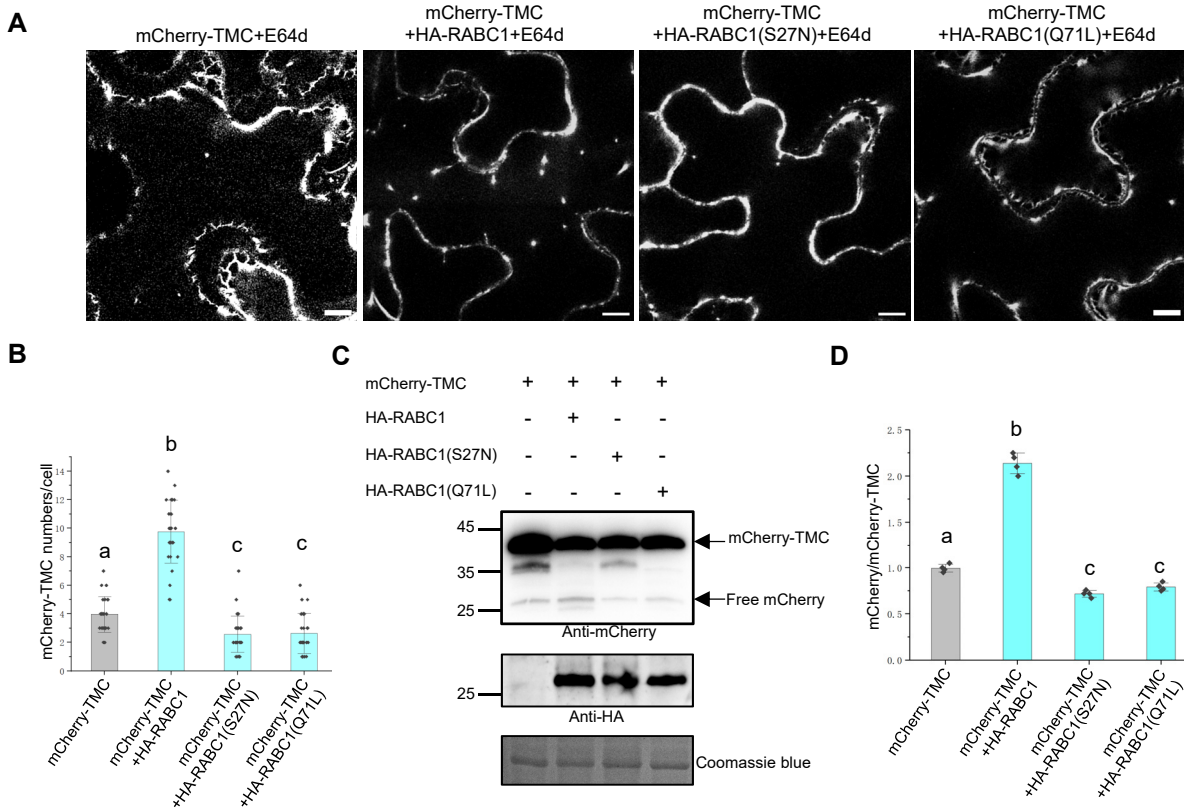


Figure S4. RABC1 promotes ER-phagy, Related to Figure 3.

- (A) Confocal images of mCherry-TMC co-expressed either alone or in combination with HA-RABC1, HA-RABC1(S27N), or HA-RABC1(Q71L). Prior to imaging, E64d was infiltrated into the samples 12 hours in advance. Scale bar = 10 μ m.
- (B) The quantification of the mCherry-TMC punctae in (A). Error bars represent means \pm SD, different letters indicate statistically significant differences (ANOVA, Fisher's least significant difference test, P<0.05).
- (C) Western blot of proteins extracted from (A) using anti-mCherry and anti-HA antibodies. Coomassie blue staining was used as the loading control.
- (D) The cleavage efficiency of free mCherry was quantified by determining the relative ratio between free mCherry and mCherry-TMC obtained from (C). Error bars represent means \pm SD, different letters indicate statistically significant differences (ANOVA, Fisher's least significant difference test, P<0.05).

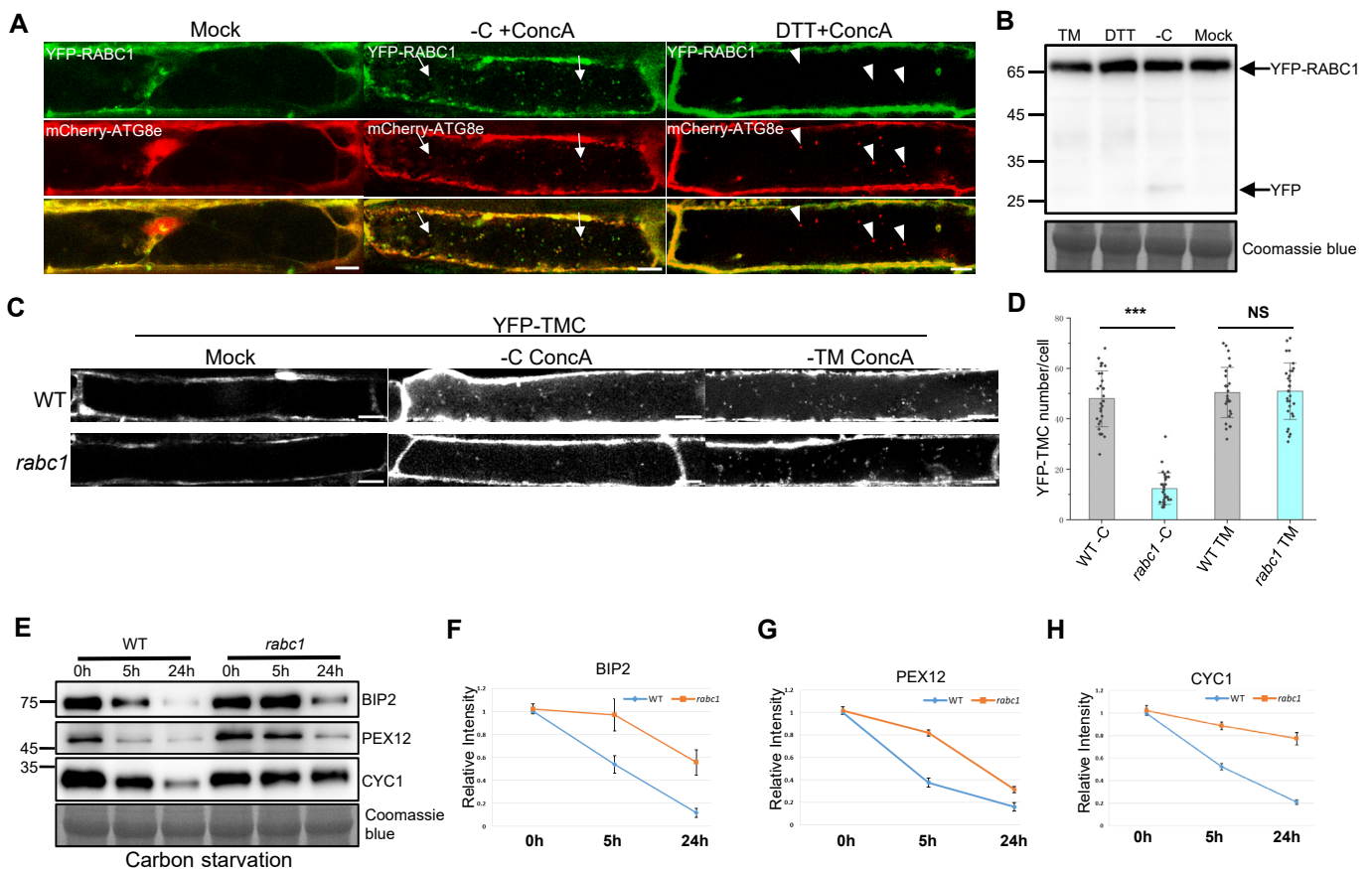


Figure S5. RABC1 is involved in autophagy triggered by carbon starvation, Related to Figure 4.
(A) Confocal images of 5-day-old seedlings expressing YFP-RABC1 and mCherry-ATG8e subjected to carbon starvation and ER stress including the mock control. The results revealed that YFP-RABC1 punctae displayed colocalization with mCherry-ATG8e within the vacuole following carbon starvation in the presence of ConcA. However, only minimal colocalization was observed between YFP-RABC1 punctae and mCherry-ATG8e during DTT-induced ER stress in the presence of ConcA. Scale bar = 10 μ m.

(B) Western blot of 5-day old *rabc1* seedlings expressing YFP-RABC1 subjected to carbon starvation, TM treatment and DTT treatment for 8 hours. Total proteins were extracted and the blot was performed with anti-GFP antibody. Coomassie blue staining was employed as the loading control.

(C) Confocal images of WT and *rabc1* mutant seedlings expressing YFP-TMC subjected to carbon starvation + ConcA, TM treatment + ConcA. Scale bar = 10 μ m.

(D) The quantification of the YFP-TMC punctae in (C). Error bars represent means \pm SD, *** represents significant difference (P -value <0.001). NS represents no significant different (P -value >0.05 , t-test).

(E) Western blot of total proteins extracted from 5 day-old WT or *rabc1* seedlings treated with carbon starvation for 0, 5, 24 hours. The blot was done with the antibodies against BIP2 (ER, row 1), PEX12 (peroxisome, row 2) and CYC1 (mitochondria, row 3). Coomassie blue staining was used as the loading control.

(F-H) The intensity of BIP2 (F), PEX12(G) and CYC1(H) protein bands in (E) quantified.

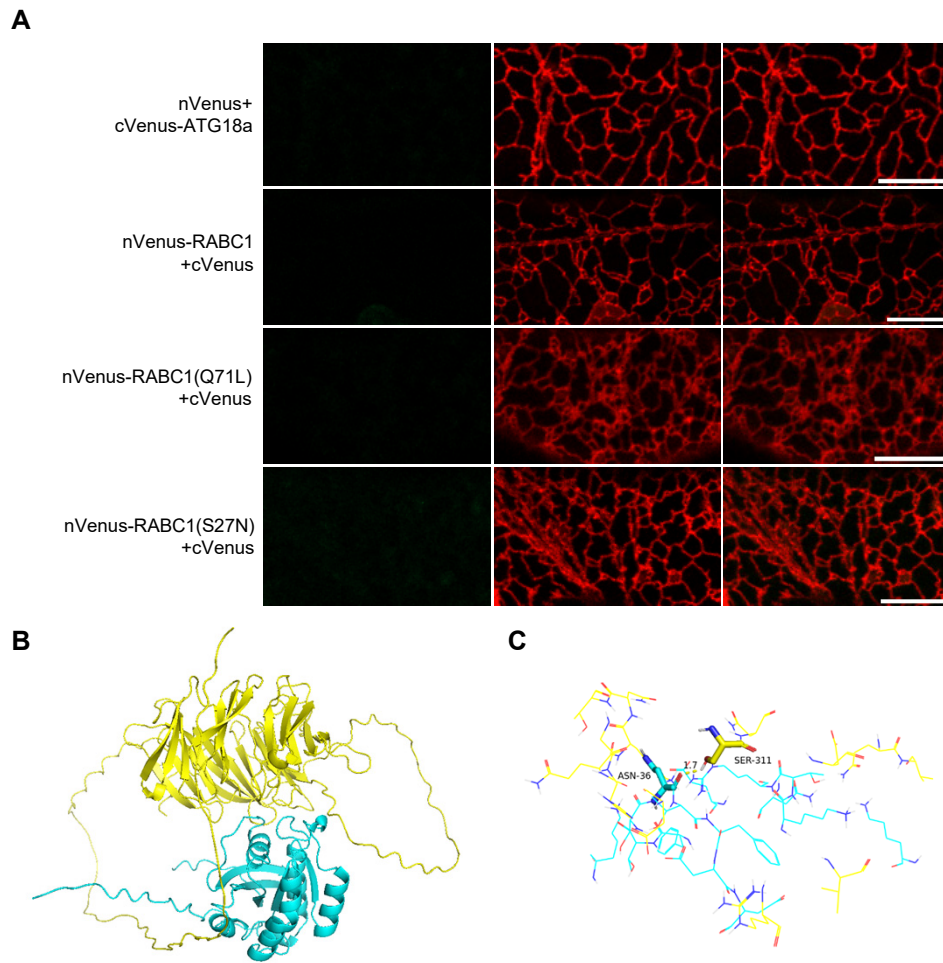


Figure S6. Controls for BiFC test and structure simulation of ATG18a-RABC1 interaction complex, Related to Figure 5.

(A) Negative controls of BiFC analysis of the interaction between ATG18a and RABC1 as indicated.

(B) The 3D view of the simulated structure generated by Hex 8.0.0. ATG18a is marked by yellow, and RABC1 is marked by blue.

(C) The interaction surface of ATG18a-RABC1. The peptides of ATG18a and RABC1 are marked by yellow and blue, respectively.

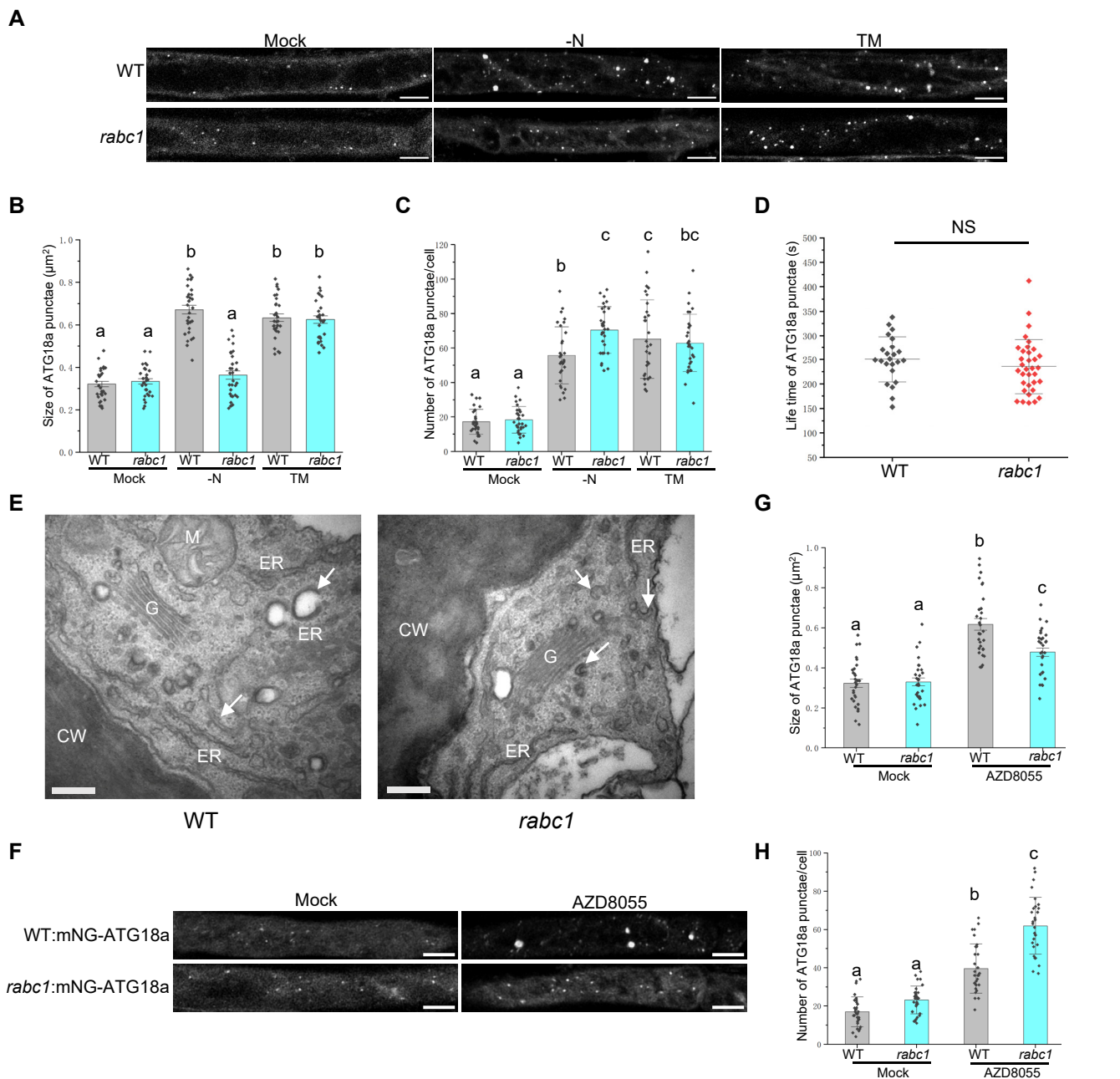


Figure S7. RABC1 participates in the expansion of autophagosomes, Related to Figure 6.

(A) Confocal images of WT and *rabc1* mutant seedlings expressing mNeonGreen-ATG18a subjected to nitrogen starvation and TM treatment for 8 hours. Scale bar = 10 μ m.

(B-C) The size (B) and number (C) of ATG18a quantified in (A). Error bars represent means \pm SD, different letters indicate statistically significant differences (ANOVA, Fisher's least significant difference test, P<0.05).

(D) Quantification of the lifetime of ATG18a-positive autophagosomes in WT and *rabc1*. There is no significant difference for the total lifetime of ATG18a in WT and *rabc1*. Error bars represent SD, NS represents no significant difference (P-value>0.05).

(E) TEM graphs of wild-type (WT) and *rabc1* mutant cells under carbon starvation. In the *rabc1* mutants, numerous unclosed autophagosomes not in the proximity to the ER (indicated by arrows) were observed. In contrast, WT cells exhibited relatively large unclosed structures close to the ER (indicated by arrows). Scale bar = 200 nm.

(F) Confocal images of WT and *rabc1* mutant seedlings expressing mNeonGreen-ATG18a subjected to AZD8055 treatment for 3 hours. Scale bar = 10 μ m.

(G-H) The size (G) and number (H) of ATG18a punctae in (F) quantified. Error bars represent means \pm SD, different letters indicate statistically significant differences (ANOVA, Fisher's least significant difference test, P<0.05).